RPSEA
Technical Report

07123-03.01

Near Miscible CO_2 Application to Improve Oil Recovery for Small Producers
07123-03

October 15, 2010

Jyun-Syung Tsau
Associate Scientist
TORP, University of Kansas
The University of Kansas Center for Research, Inc.
2385 Irving Hill Road, Lawrence, KS 66045-7563

LEGAL NOTICE

This report was prepared by *University of Kansas Center for Research, Inc.* as an account of work sponsored by the Research Partnership to Secure Energy for America, RPSEA. Neither RPSEA members of RPSEA, the National Energy Technology Laboratory, the U.S. Department of Energy, nor any person acting on behalf of any of the entities:

a. MAKES ANY WARRANTY OR REPRESENTATION, EXPRESS OR IMPLIED WITH RESPECT TO ACCURACY, COMPLETENESS, OR USEFULNESS OF THE INFORMATION CONTAINED IN THIS DOCUMENT, OR THAT THE USE OF ANY INFORMATION, APPARATUS, METHOD, OR PROCESS DISCLOSED IN THIS DOCUMENT MAY NOT INFRINGE PRIVATELY OWNED RIGHTS, OR

b. ASSUMES ANY LIABILITY WITH RESPECT TO THE USE OF, OR FOR ANY AND ALL DAMAGES RESULTING FROM THE USE OF, ANY INFORMATION, APPARATUS, METHOD, OR PROCESS DISCLOSED IN THIS DOCUMENT.

THIS IS A TECHNICAL REPORT. THEREFORE, ANY DATA, CALCULATIONS, OR CONCLUSIONS REPORTED HEREIN SHOULD BE TREATED AS PRELIMINARY.

REFERENCE TO TRADE NAMES OR SPECIFIC COMMERCIAL PRODUCTS, COMMODITIES, OR SERVICES IN THIS REPORT DOES NOT REPRESENT OR CONSTIITUTE AND ENDORSEMENT, RECOMMENDATION, OR FAVORING BY RPSEA OR ITS CONTRACTORS OF THE SPECIFIC COMMERCIAL PRODUCT, COMMODITY, OR SERVICE.

Abstract

This technical report discusses fundamental studies of phase behavior for the CO_2/crude oil system and the displacement process at near miscible conditions which are at pressures below but near the minimum miscibility pressure (MMP) at reservoir temperature.

Phase behavior studies between CO_2 and Arbuckle crude oil were carried out to define near miscible conditions at reservoir conditions. Swelling/extraction tests combined with slim-tube experiments were interpreted to identify the mass transfer mechanisms at near miscible condition. A phase behavior model was developed to match PVT data and MMP in the slim-tube experiment. Good agreement was obtained between simulated and observed data from slim-tube experiments. Core flooding tests were conducted to evaluate oil recovery at near miscible condition at which pressure varies from 1350 psi (MMP) to 1150 psi. Recovery of over 50% of the waterflood residual oil saturation was observed when CO_2 was used to displace Arbuckle oil from Berea, Baker dolomite and Arbuckle dolomite cores.

At near miscible conditions, extraction appears to be the primary mechanism for mass transfer between hydrocarbon components and CO_2. However, the reduction of oil viscosity by a factor of five occurred when CO_2 dissolved in the oil. This suggests that some of the additional oil recovery may be attributed to reduction of the mobility ratio between CO_2 and resident oil.

The phase behavior model developed in this study is to be used in a reservoir model to simulate CO_2 injection process at near miscible condition for a target reservoir. If the process proves successful, the benefits will be increase of domestic production for small producers as well as significant increase of the resource base for CO_2 flooding and sequestration.

THIS PAGE INTENTIONALLY LEFT BLANK

TABLE OF CONTENTS

	Page
Table of Contents	i
List of Tables	ii
List of Figures	iii
1. Introduction	1
Background Information	1
2. Task 4.1 Slim-tube Experiments	3
Experimental Setup and Specifications	4
Experimental Procedures	6
Results and Discussions	7
Summary	9
3. Task 4.2 Phase Behavior Studies on CO_2/Crude Oils	10
Swelling/Extraction Tests	10
Experimental Setup and Specifications	10
Experimental Procedures	12
Experimental Principles	13
Apparatus Validation	14
Effect of System Pressure	15
Effect of System Temperature	17
Viscosity Measurements	19
Estimation of MMP	23
Summary	25
4. Task 4.3 Phase Behavior Model	26
Equation of State	26
Phase Behavior Modeling using WINPROP	27
Slim-tube Experiment Modeling using GEM	31
Summary	32
5. Task 4.4 Flow Tests with Core Samples at Near Miscible Conditions	33
Characterization of Core Samples	35
Gravimetric Method	35
Tracer Tests	35
Core Floods Experimental Setup	38
Experimental Procedures	39
Results and Discussions	39
Secondary CO_2 Flooding	40
Tertiary CO_2 Flooding	41
Summary	45
6. Conclusions	46
References	47

List of Tables

		Page
Table 1	Physical property of Ogallah crude oil and the lumped heavy component C36+3 ……	3
Table 2	Slim-tube characteristics ……	5
Table 3	Phase equilibrium data of CO_2/n-decane at 71.1^oC ……	14
Table 4	Adjustments of EOS parameters ……	29
Table 5	Maximum percentage errors between simulated and experimental data …….	31
Table 6	Slim tube model properties ……	31
Table 7	Density/Viscosity of Brine at 86^oF/110^oF …….	34
Table 8	Core plug properties ……..	40
Table 9	Tertiary CO_2 flood results of Berea sandstone …….	44
Table 10	Tertiary CO_2 flood results of Arbuckle dolomite …….	44
Table 11	Tertiary CO_2 flood results of Baker dolomite ……..	44

List of Figures

		Page
Figure 1	Ogallah unit, Trego County, Kansas …….	2
Figure 2	GC compositional analysis result of Ogallah crude oil ……	3
Figure 3	Schematic of slim tube setup …….....	4
Figure 4	Minimum miscibility pressure determinations at 110°F and 125°F…….	8
Figure 5	Near miscible region for Ogallah crude oil at 110°F ……	8
Figure 6	Density profile of the effluent at 110°F ……	9
Figure 7	Schematic of swelling/extraction test apparatus setup …….	10
Figure 8	Image of the swelling/extraction experimental setup …….	11
Figure 9	Comparison of liquid phase compositions for CO_2+ n-decane system at 71.10^{o}C ……	13
Figure 10	Change of initial oil volume with pressure ……	10
Figure 11	Effect of pressure on CO_2 solubility and swelling factor at 110°F …….	11
Figure 12	Effect of temperature on CO_2 solubility …….	12
Figure 13	Effect of temperature on Swelling/ Extraction curves ……..	13
Figure 14	Schematic of high-pressure viscosity measurement setup …….	14
Figure 15	Image of the high-pressure viscosity measurement setup ……..	15
Figure 16	High pressure generator …….	21
Figure 17	Effect of pressure on Ogallah oil viscosity at 110°F …….	23
Figure 18	Viscosity of crude oil saturated with CO_2 at 110°F ……	23
Figure 19	Estimation of MMP from extraction test of Ogallah crude oil ……	24
Figure 20	Comparison of viscosity/density experimental data and simulated data ……	30
Figure 21	Comparison of saturation pressure/swelling factor experimental and simulated data ……..	30
Figure 22	Comparison of simulated MMP and experimental MMP ……..	32
Figure 23	Vacuum and saturation setup ……	34
Figure 24	Estimation of pore volume from tracer tests ……	36
Figure 25	Schematic of tracer test setup ……..	37

Page

Figure 26 Schematic of core flood setup …….. 38

Figure 27 Comparison of oil recovery between slim-tube and core flooding experiment ……. 41

Figure 28 Effluent profile of production fluid during CO_2 flooding at 1317 psig and 110°F ……. 42

Figure 29 Effect of rock type on recovery efficiency at 110°F …… 43

Figure 30 Effect of water saturation on oil recovery efficiency at 110°F …… 45

1. Introduction

This project describes a research program to evaluate and enhance the application of CO_2 displacement at near miscible pressures for improved oil recovery (IOR) and carbon sequestration for small producers. The main objectives are 1) to define the near miscible region where oil recovery efficiency improves significantly over the immiscible region in CO_2 flooding, 2) to investigate the feasibility of near miscible CO_2 flooding for IOR, and 3) to evaluate the potential for carbon sequestration at near miscible conditions in the Arbuckle formation in Kansas. Satisfactory completion of the program would permit the assessment of the effectiveness of CO_2 displacement at near miscible pressures which are below minimum miscibility pressure (MMP), and make it possible to determine the potential of CO_2 flooding and carbon sequestration in relatively shallow reservoirs. A target reservoir, the Arbuckle formation of Kansas, Ogallah unit was used in this research for study. The field operating pressure is generally about 200 psi below MMP. Attainment of the research objectives would make this resource available to CO_2 displacement and carbon sequestration.

Two technical reports are prepared at the completion of this project. The first technical report discusses fundamental studies of phase behavior for the CO_2/crude oil system and the displacement process at pressures near the MMP. The second technical report describes the construction of geo-model and simulation results of reservoir model with a commercial simulator, and discusses the improvement of oil recovery by CO_2 injection and the potential for carbon sequestration in oil reservoirs at near miscible conditions.

In this technical report, the description of experiments and results is divided into four sections corresponding to four subtasks as defined in proposed research project. Specific subtasks are: 1) perform slim-tube experiments, 2) conduct swelling/extraction tests on CO_2/oil mixtures, 3) construct a phase behavior model, and 4) conduct core flow tests at near miscible conditions.

Background Information

The target oil field, Ogallah unit is located at Trego County, Kansas (as shown in Figure 1). The unit is currently operated by Carmen Schmitt, Inc. The unit produces from Arbuckle formation (3950-4060 ft). Reservoir temperature ranges from 92°F to 130°F with an average

temperature of 110 ^{o}F. Active water drives have maintained reservoir pressure at approximately 1150 psi.

The stock tank oil collected from tank battery from Ogallah unit was used for all the experiments. The crude oil was centrifuged at the rate of 2000 rpm for at least an hour to separate water, oil and solid particles. Two layers of glass microfibre filters with the size of 1.6 micron and 1 micron were used respectively to filter the crude oil.

A compositional analysis of the crude oil using Gas Chromatography (GC) technique is shown in Figure 2. Percentage of asphaltenes (heptane insolubles) in this crude oil was determined approximately 0.93 % based on ASTM D 893-85. Carbon dioxide in use was purchased through commercial vender with 99.99% of purity. Table 1 summarizes the physical properties of the oil and the lumped heavy component C36+.

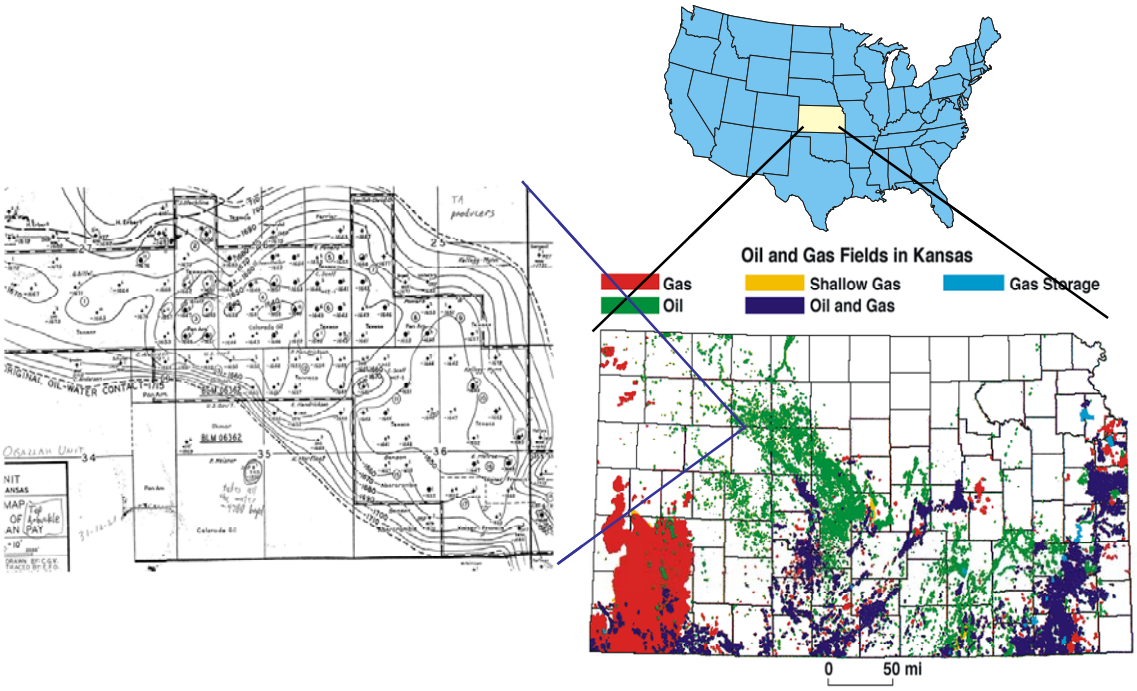

Figure 1 Ogallah unit, Trego County, Kansas

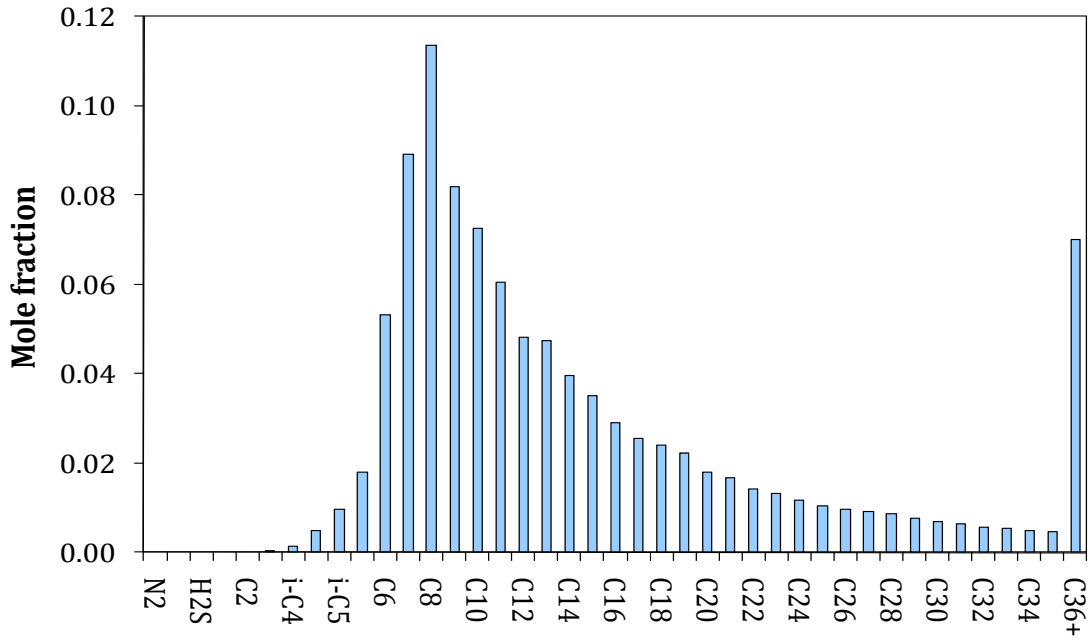

Figure 2 GC compositional analysis result of Ogallah crude oil

Table 1 Physical property of Ogallah crude oil and the lumped heavy component C36+

Molecular Weigh, g/mol	228.71
API	33.34
Density @ 14.7 psi & 60°F, g/cc	0.8584
Viscosity @ 14.7 psi & 60°F, cp	13.4
C36+ molecular weight, g/mol	873.24
C36+ density @ 14.7 psi & 60°F, g/cc	0.9978

2. Task 4.1 Slim-tube experiments

Minimum miscibility pressure was determined by performing displacement experiments in a 40-foot slim tube. The lowest pressure at which oil recovery reaches 90% at 1.2 HCPV CO_2 injections is defined as the MMP. A series of slim-tube experiments were run at a suitable pressure increment starting at 80% of MMP to define the near miscible pressure range.

Dead oil samples collected from Arbuckle reservoirs was used in the experiments. Mixture density was measured using an in-line densitometer while the viscosity was measured with a high pressure viscometer independently.

Completion of this task provided the data required to characterize the near miscible condition. These results include the oil recovery performance, phase density and viscosity of CO_2/oil mixtures as a function of pressure.

Experimental Setup and Specifications

The basis of slim tube tests is that the small-diameter tube filled with an unconsolidated porous medium serves as an idealized medium for CO_2 and crude oil to contact and develop dynamic miscibility. Non-idealities such as viscous fingering and gravity effect are ignored because of the large length to diameter ratio in slim tube configuration. Oil recovery is therefore attributed to the thermodynamic phase behavior. The recovery performance at different pressures can be used to determine the MMP. Slim tube tests have not only been used to determine reservoir candidates for miscible processes but also widely used for fine tuning the reservoir simulator.

In this study, a number of slim tube displacements were conducted for a range of pressures, holding the temperature constant at the reservoir temperature (110^oF-125^oF) to determine the MMP of this system. An oil recovery factor of at least 90% at 1.2 HCPV of CO_2 injected is used to define the MMP of the system.

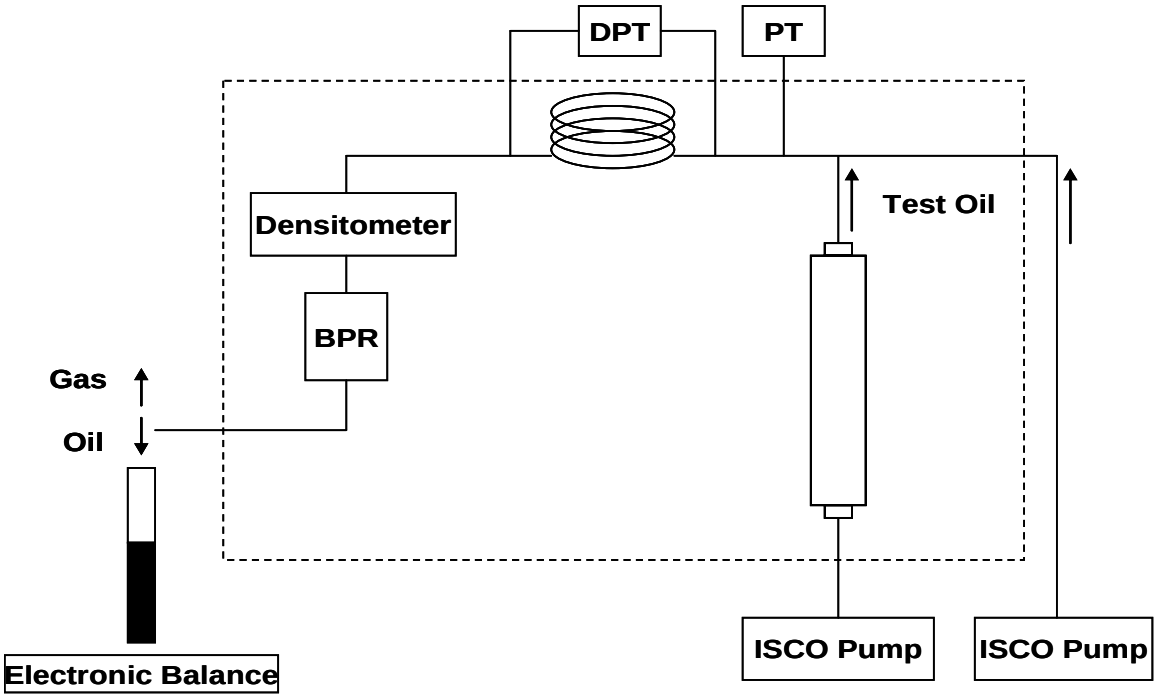

Figure 3 Schematic of slim tube setup

Schematic of the slim tube setup is shown in Figure 3. The system temperature is controlled and maintained in a Lindberg/Blue M oven with Eurotherm temperature controller. The system pressure is controlled and maintained by a back pressure regulator at the outlet. Back pressure regulator models BPR-50 is a dome-load type, which controls the upstream pressure at a setting pressure applied to the dome. It is designed to operate using compressed gas in the dome and water, oil, gas in the body. A high pressure bottle of inert gas, such as nitrogen, is required to pressurize the unit. The back pressure regulator has a working pressure of 5000 psi at 200°F.

Three Valydine pressure transducers are installed to measure pressures at different locations, such as pressure drop across the slim tube, upstream pressures (CO_2/oil pressure), and downstream pressure (back-pressure regulator pressure). The transducers have the capability of measuring pressures up to 2500 psi with the accuracy of 0.25% of their full scale (0-2500 psi).

The injection system consists of two Isco, Inc. 260DM syringe pumps (for CO_2/crude oil transfer and injection at a desired rate) and a transfer cylinder (for crude oil storage). The capacity of the transfer cylinder is 485 cc. The cylinder can withstand a maximum pressure of 3000 psi.

The slim tube consists of a coiled 38.29 ft-long stainless steel tube with an ID of 0.24 in. packed with glass beads. Slim tube properties were listed in Table 2.

Table 2 Slim tube characteristics

Length, ft	38.29
O.D, in	0.31
I.D, in	0.24
Porosity	0.37
Bulk volume, cc	347.8
Pore volume, cc	127.76
Permeability, mD	4900
Packing beads	No. 2024

Density of the effluent is measured continuously by an inline densitometer. The densitometer consists of two units. The DPRn 422 density transducer measures the characteristic frequency of vibration. The Anton Paar mPDS 2003V3 Evaluation unit translates the

characteristic frequency of vibration into a density value. The measuring range is 0-3g/cc within the temperature range of -13°F – 257°F and the pressure range of 0-2900 psi.

Effluent is continuously flashed to atmospheric conditions. The separator gas is connected to a flow meter. The separator liquid is collected in a graduated cylinder. The graduated cylinder is placed on an electronic balance which is connected to the data acquisition system.

Experimental Procedures

At least 2 PV of methylene chloride followed by 2 PV of mineral oil were injected to clean the slim tube prior to the experiment. The slim tube was then saturated with at least 2 PV of crude oil at the desired temperature. While the slim tube was being saturated with crude oil, the system was pressurized gradually to the desired operating pressure using the back pressure regulator. Upstream pressure changed accordingly to the pressure of the back pressure regulator as it was set. To prevent pressure from one side of the diaphragm of the back pressure regulator from becoming significantly higher than the pressure on the other side and damage the diaphragm, it was necessary to pressurize the system slowly, for example, 0-100 psig, switch off the gas supply valve and wait for the upstream pressure to catch up with the downstream pressure. Once the desired pressure was reached, the system was allowed to equilibrate under pressure. Pressure of the CO_2 pump was set slightly above the pressure of the back pressure regulator. Temperature of the pump was set at temperature of the system. CO_2 flow rate was set at a constant of 0.05cc/min. This corresponds to a Darcy velocity of 8 ft/day.

A log file was created to record the following parameters: temperature of the system, pressure of the system (back-pressure regulator pressure/downstream pressure), upstream pressures (CO_2/oil pressure), pressure drop across the slim tube, weight of the separator liquid, and separator gas flow rate. The initial and final volumes of CO_2 in the pump were recorded manually.

The experiment was terminated when at least 1.2 HCPV of CO_2 at the temperature and pressure of the pump were injected. The system was depressurized by venting the dome load gas slowly. Residual oil in the slim tube was removed by following the same cleaning procedure as mentioned earlier. The entire experiment was then repeated several times at different pressures holding other variables constant.

Results and Discussions

Slim tube displacements were conducted at 110°F and 125°F representing the range of temperatures reported from the field. The effluent was observed when it was flashed to the atmosphere during the displacement. A gradual change of color of the flowing fluid from the oil to clear gas was observed for pressures above MMP. Two-phase flow was observed for pressures below MMP. Gas breakthrough was seen earlier from displacements at pressures below MMP compared with displacements at pressures above MMP.

Percentage of oil recovery was calculated as follows:

$$\%\ oil\ recovery = \frac{Weight\ of\ oil\ produced}{Pore\ Volume \times Oil\ density} \times 100\%$$

Pore volume (PV) of CO_2 injected was calculated as follows:

$$PV = \frac{time \times CO_2\ flow\ rate}{Pore\ Volume}$$

Percentage of oil recovery at 1.2 PV of CO_2 injected was plotted against slim tube average pressure to determine the MMP of the system at 110°F and 125°F, as shown in Figure 4. MMP of the system were estimated to be 1350 psig at 110°F and 1650 psig at 125°F. As expected, MMP increases with increasing temperature. This phenomenon is closely related to the dependence of CO_2 density on temperature and pressure and is explained in detail in the discussion of the next experiment.

Slim tube results indicated that miscibility was not achievable at the current reservoir pressure of 1150 psig; however, the recovery efficiency was relatively high, 78% - 83% of the original oil in slim tube for a temperate range of 110°F to 125°F and at 1150 psig.

Since the MMP of this oil was determined to be 1350 psig at 110°F and the near miscible range was selected from 0.8MMP to MMP in this study, the near miscible region for this particular oil is defined from 1100 psig to 1350 psig at 110°F (Figure 5).

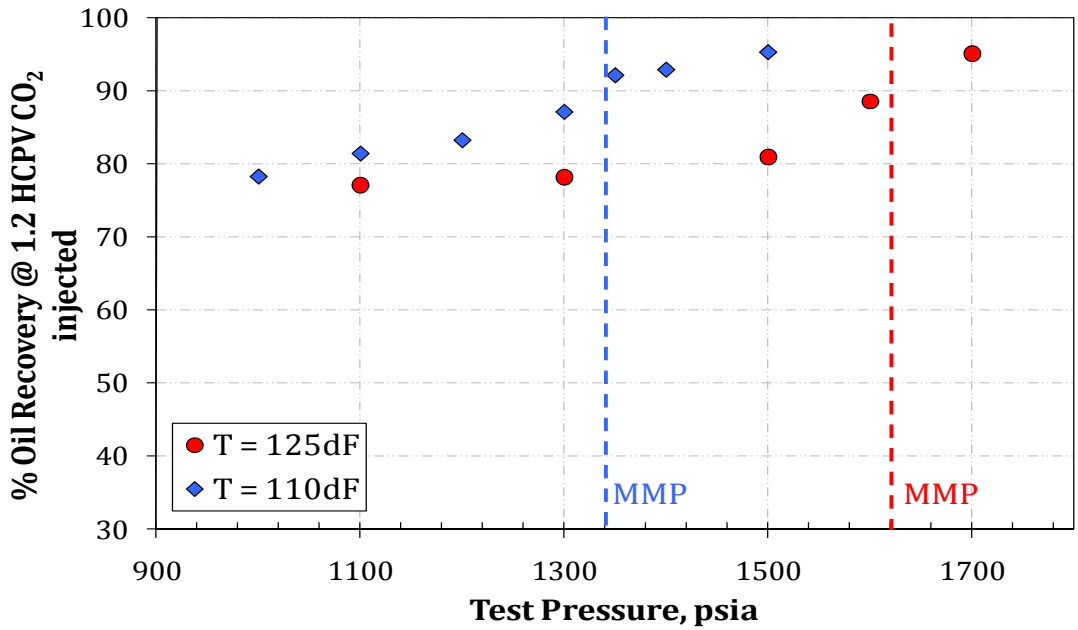

Figure 4 Minimum miscibility pressure determinations at 110°F and 125°F

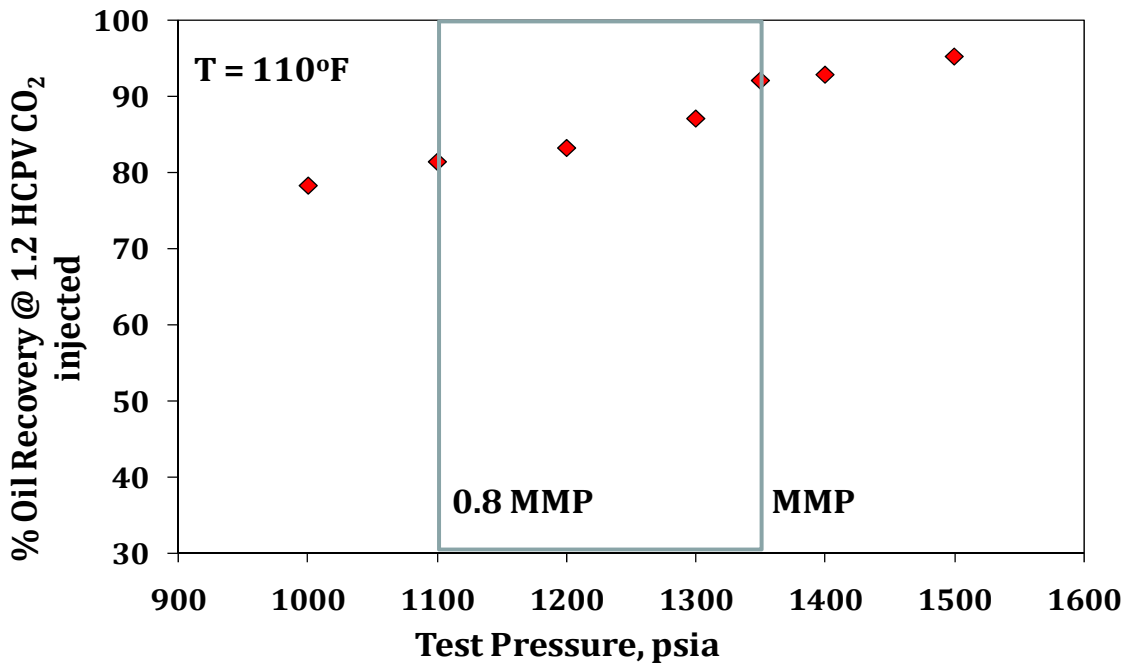

Figure 5 Near miscible region for Ogallah crude oil at 110°F

Figure 6 shows the density profile of the effluent at pressures below MMP. Prior to the breakthrough of CO_2 the effluent density was equal to the oil phase density (0.834 g/cc) at

reservoir temperature and slim-tube average pressure. The abrupt change in density of the effluent corresponds to the breakthrough of CO_2. Significant reduction of effluent density occurred at pressures below MMP following CO_2 breakthrough. After breakthrough of CO_2, average densities of the effluent were 0.434, 0.535 g/cc at average pressures of 1100, 1200 psig. At the same pressure and temperature, the densities of pure CO_2 are 0.221 g/cc and 0.275 g/cc. The increase of density in the effluent profile is evidence that light hydrocarbon components from the oil continued to be vaporized or extracted by CO_2 contributing to relatively high recovery efficiencies for near miscible CO_2 displacement.

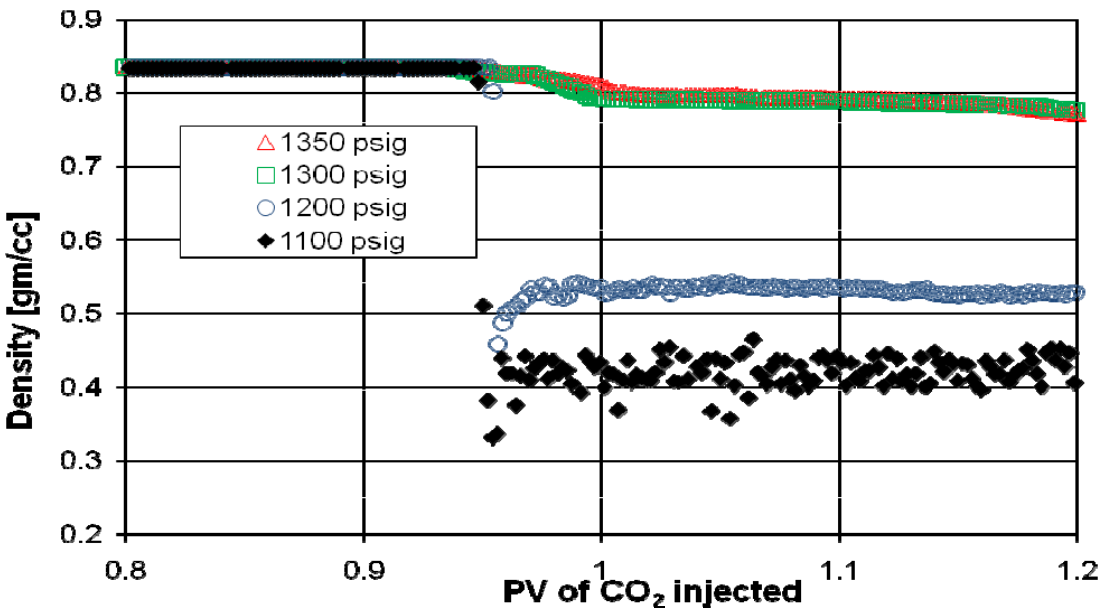

Figure 6 Density profile of the effluent at 110°F

Summary

1) The MMP was estimated to be 1350 psig at 110°F and 1650 psig at 125°F.
2) Miscibility is not achievable at the current reservoir pressure of 1150 psig.
3) The near miscible pressure conditions to be investigated in core flow test is defined from 1100 to 1350 psig.
4) At the current reservoir pressure of 1150 psig and at a temperature range of 110°F to 125°F, the recovery efficiency of the original oil in place from slim tube experiment varied from 78 to 83% which is attributed to mass transfer mechanism between crude oil and carbon dioxide during the displacement process.

3. Task 4.2 Phase Behavior Studies on CO_2/Crude Oils

Swelling tests were performed to determine the relationship between saturation pressure, swelling factor and CO_2 volume injected. Extraction tests were conducted to examine extraction of liquid hydrocarbon into a CO_2-rich phase and the effect of pressure on the extraction.

Completion of this task allowed us to examine the phase behavior at near miscible conditions independently from slim-tube experiments, and to identify characteristics of phase behavior in a displacement process.

Swelling/Extraction Tests

Swelling/extraction tests were performed to examine the oil recovery mechanisms in the near-miscible region and to provide data to tune the phase behavior model. Swelling tests were conducted to determine the relationship between saturation pressure, swelling factor and CO_2 volume injected. Extraction tests were carried out to examine the extraction of liquid hydrocarbon into a CO_2-rich phase and the effect of pressure on the extraction.

Experimental Setup and Specifications

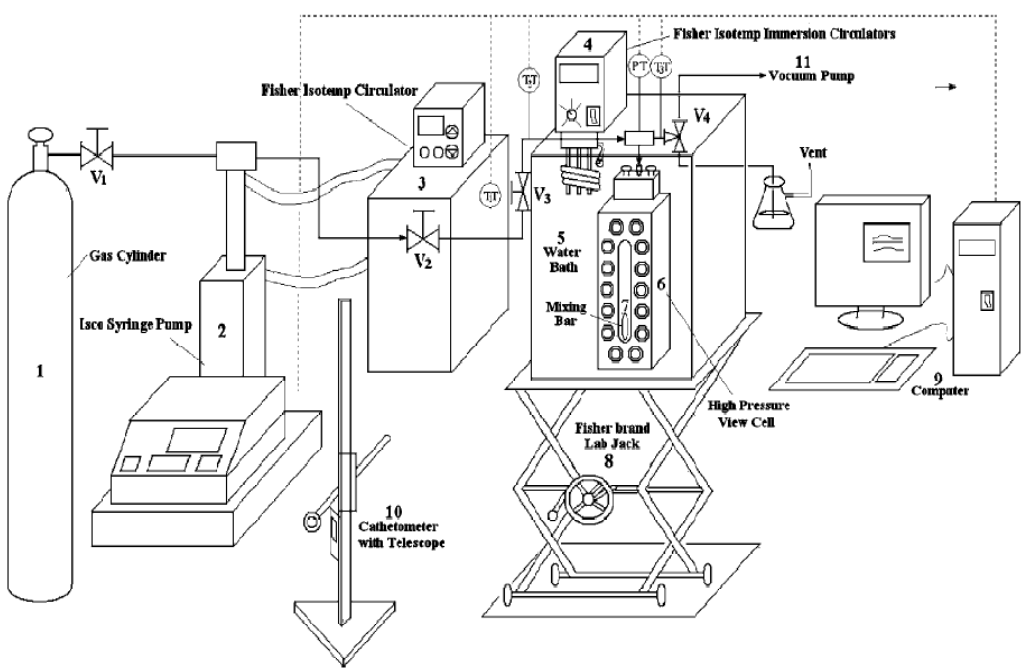

Figure 7 Experimental setup include (1) Gas cylinder (2) Isco Syringe pump (3) Fisher Isotemp circulator (4) Fisher Isotemp Immersion circulator (5) water bath (6) high pressure view cell (7) mixing bar (8) laboratory jack (9) computer (10) cathetometer with telescope (11) vacuum pump (Ren *et al.*, 2008)

The schematic of swelling/extraction setup and its image are shown in Figure 7 and Figure 8. An Isco, Inc. 100DM syringe pumps is used for CO_2 injection. Temperature of the pump is controlled by a Fisher, Inc. Isotemp circulator, model 3016 and measured by an Ertco-Eutechnic 5 digit thermister, model 4400 in the range of 0-100°C.

The gas lines are heated using fiberglass covered heating tape, controlled by two variable AC transformers, Staco Energy model 3PN1010B. Temperature of the gas lines is measured using T-type thermocouples. Fiberglass cloth tape is used to prevent heat dissipation to the surroundings.

The key component of this setup is the high pressure view cell with high pressure gauge glass window allowing visual observations of fluids under experimental conditions. The view cell is made of stainless steel and has a volume of 26 cc. The gauge glass window allows a maximum temperature of 280°C and pressure of 4000 psi. Pressure in the view cell is measured by a 5000 psi Heise DXD Series 3711 precision digital pressure transducer. A 3.2mm diameter × 12.7 mm PTFE coated stir bar is placed inside the view cell. Mixing is achieved by an external rare-earth magnet in a slot behind the cell raised and lowered by a pulley system.

The view cell is immersed into the water bath by raising/lowering the platform jack. The temperature of the water bath is adjusted by an immersion circulator Haake DC30/DL3 and a Fisher, Inc. Isotemp circulator, model 3016. An Eberbach 5160 cathetometer is used to measure the height of the liquid in the view cell.

Figure 8 Image of the swelling/extraction experimental setup

Experimental Procedures

The pump was filled with CO_2. Temperature of the pump was set constant and above the critical temperature of CO_2 (31.1^oC). Pressure of the pump was set constant at the maximum anticipated pressure. The pump automatically adjusted the volume of CO_2 to achieve constant temperature and pressure. Temperature of the gas lines was set at temperature above the critical temperature of CO_2 to avoid CO_2 condensation inside the lines. Temperature of the water bath was set constant at the desired temperature.

A predetermined volume of crude oil was carefully injected into the view cell to avoid liquid droplets on the wall of the view cell. The view cell was attached to the gas lines and then immersed into the water bath.

When the whole system was thermally equilibrated, the gas lines and the view cell were quickly flushed with CO_2 at low pressure to remove any residual gas or air.

A log file was created to record the following parameters: the pump condition (temperature, pressure and volume of CO_2), the temperature of the gas lines, the view cell condition (temperature and pressure). The height of the liquid sample in the view cell was recorded manually. Initially conditions were also recorded manually.

The cell pressure was increased in discrete steps by CO_2 injection from the top of the view cell. CO_2 injection was stopped when a desired pressure was achieved. CO_2 flow rate was kept slowly so that there was no PVT disturbance. This was done by checking the pump pressure frequently to make sure the pump pressure did not drop too much from the set pressure. Final volume of CO_2 in the pump was recorded when CO_2 flow rate is read zero.

During pressurization process, the time required for the contents in the view cell to equilibrate under a particular pressure and temperature is minimized by magnetically stirring. At that time, the following parameters were recorded manually: the height of the liquid sample in the view cell, the pump condition (temperature, pressure & final volume of CO_2), temperature of gas lines and the view cell condition (temperature & pressure).

At the end of test, the view cell was cleaned with methylene chloride, acetone solution and blown dry with compressed air.

Experimental Principles

The phase equilibria data were obtained based on a mass balance and the following assumptions: 1) the pressure of CO_2 is much greater than the vapor pressure of the crude oil and 2) vapor phase composition of the hydrocarbon component is much less than CO_2

The mass balance equation of CO_2 is as follows:

$$m_g = m_{pump} - m_{lines} - m_{headspace} + m^o{}_{lines} + m^o{}_{headspace}$$

$$m_{pump} = \Delta V_{pump}\rho(T_{pump}, P_{pump})$$

$$m_{lines} = \Delta V_{lines}\rho(T_{lines}, P)$$

$$m_{headspace} = \Delta V_{headspace}\rho(T, P) = \left(V_{cell} - V_{liquid}\right)\rho(T, P)$$

$$m^o{}_{lines} = \Delta V_{lines}\rho(T_{lines}, P^o)$$

$$m^o{}_{headspace} = \Delta V_{headspace}\rho(T, P^o) = \left(V_{cell} - V_{liquid}\right)\rho(T, P^0)$$

Where

m_g : the mass of CO_2 dissolved in the liquid

m_{pump} : equal to the product of volume of CO_2 displaced from the pump and density of CO_2 at the pump constant temperature & pressure

m_{lines} : the product of volume of the lines and density of CO_2 at temperature of the lines & system equilibrium pressure

$m^o{}_{lines}$: the product of volume of the lines and density of CO_2 at temperature of the lines & system initial pressure

$m_{headspace}$: the product of volume of the headspace and density of CO_2 at temperature & pressure of the equilibrium system. The volume of the headspace is the difference between volume of the cell and volume of the liquid in the cell.

$m^o{}_{headspace}$: the product of volume of the headspace and density of CO_2 at temperature & pressure of the initial system. The volume of the headspace initially is the difference between volume of the cell and initial volume of the liquid in the cell.

CO_2 density was calculated using REFROP database which used the ultra-accurate Span-Wagner equation of state. Mole fraction of CO_2 in the liquid phase was calculated as follows:

$$x_g = \frac{n_g}{n_g + n_l} = \frac{m_g / M_g}{m_g / M_g + m_l / M_l}$$

Apparatus Validation

The apparatus was verified by comparing experimental data obtained from this apparatus with literature data for n-decane/CO_2 mixture at 71.1^oC by Ren *et al.* (2008). The experimental data had excellent agreement with the literature data obtained from different experimental methods. Phase equilibrium data of CO_2/n-decane at 71.1^oC was obtained and shown in Table 3.

Table 3 Phase equilibrium data of CO_2/n-decane at 71.1^oC

Run 1		Run 2	
Pressure, psi	x_{CO2}	Pressure, psi	x_{CO2}
192.18	0.09609	209.43	0.10900
425.25	0.21070	434.97	0.22498
701.98	0.34940	643.68	0.32669
1005.55	0.50260	866.89	0.44391
1270.24	0.61657	1080.39	0.52821
1448.35	0.69121	1321.58	0.64927
1531.45	0.72330	1495.77	0.71555
1666.05	0.77723	1612.38	0.76148
		1709.41	0.80048
		1771.35	0.82829

Analysis of this data was based on the assumption that the amount of liquid component in the vapor phase is negligible. Although the composition of the vapor phase was not actually analyzed in our experiments, it had been demonstrated earlier by Ren *et al.* (2008) that the percentage of n-decane in CO_2 vapor phase was less than 0.13%. Figure 9 shows that the p-x phase equilibrium of CO_2/n-decane generated using this apparatus were reproducible and in excellent agreement with literature data, Nagarajan *et al.* (1986) and Jennings *et al.* (1996), and therefore, it could be used for crude oil/CO_2 system.

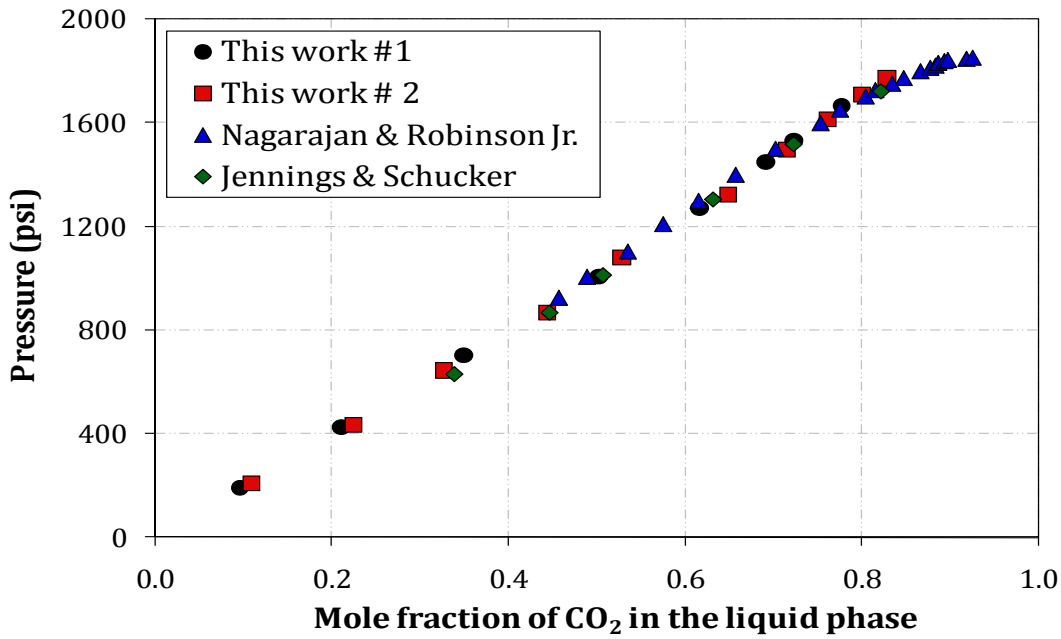

Figure 9 Comparison of liquid phase compositions for CO_2+ n-decane system at 71.10°C (160°F) with literature data (○) this work (□) this work (Δ) Nagarajan & Robinson Jr. (◊) Jennings & Schucker

Effect of System Pressure

Figure 10 illustrates the observations of Ogallah oil/CO_2 phase behavior in the view cell. The volume of oil in the liquid phase increases with the increasing pressure (P_1) as CO_2 dissolves in and swells the oil. As the pressure (P_2) further increases, CO_2 density increases. Since the ability of CO_2 to extract hydrocarbon components from crude oil is enhanced as its density increases with the pressure, CO_2 starts extracting hydrocarbons from the crude oil. The volume of oil in the liquid phase is reduced at pressure above P_1 as the rate of extraction becomes greater than the rate of swelling.

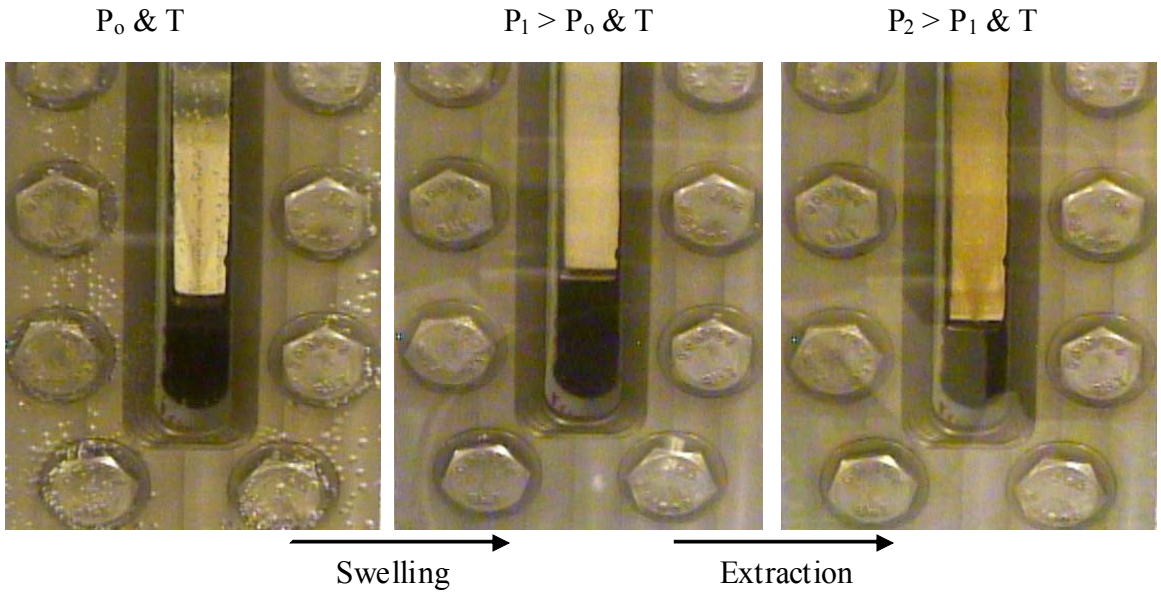

Figure 10 Change of initial oil volume with pressure

Figure 11 shows the swelling/extraction curve for Ogallah/CO_2 system at 110°F with the sample size of 3 cc. The sample volume was about 12 % volume of the view cell. The swelling factor (SF) of oil is the ratio of liquid volume at test pressure divided by the liquid volume at atmospheric pressure and at 110°F. This value is determined by measuring the change of the interface level as a result of CO_2 dissolution in the oil or as a result of hydrocarbon extracted into the CO_2 rich vapor phase. Swelling factor was equal to 1 at initial conditions. As a result of CO_2 dissolution into the liquid phase, the liquid phase swelled and the swelling factor was greater than 1. Maximum swelling occurred at 1158 psi, when volume of the liquid phase became 1.21 of its original volume with 0.728 mole fraction of CO_2 dissolved in the liquid phase. Major extraction started at approximately 1158 psi. As pressure increased, hydrocarbon components of the crude oil were removed from the liquid phase, the liquid phase shrank and swelling factor was reduced. At 2035 psi, the volume of CO_2 rich liquid phase shrank as much as 39.2 % of its original volume. CO_2 solubility is also plotted in Figure 11 as a function of pressure up to 1158 psi. Calculations of CO_2 solubility at pressures above 1158 psi are invalid since the assumption that the components of the liquid phase do not vaporize does not hold true. In the pressure range from 1100 psig to 1350 psig which is within 0.80 MMP, the extraction or vaporization of

hydrocarbon components from crude oil appears to be the primary mechanism in phase behavior between the interaction of CO_2 and oil.

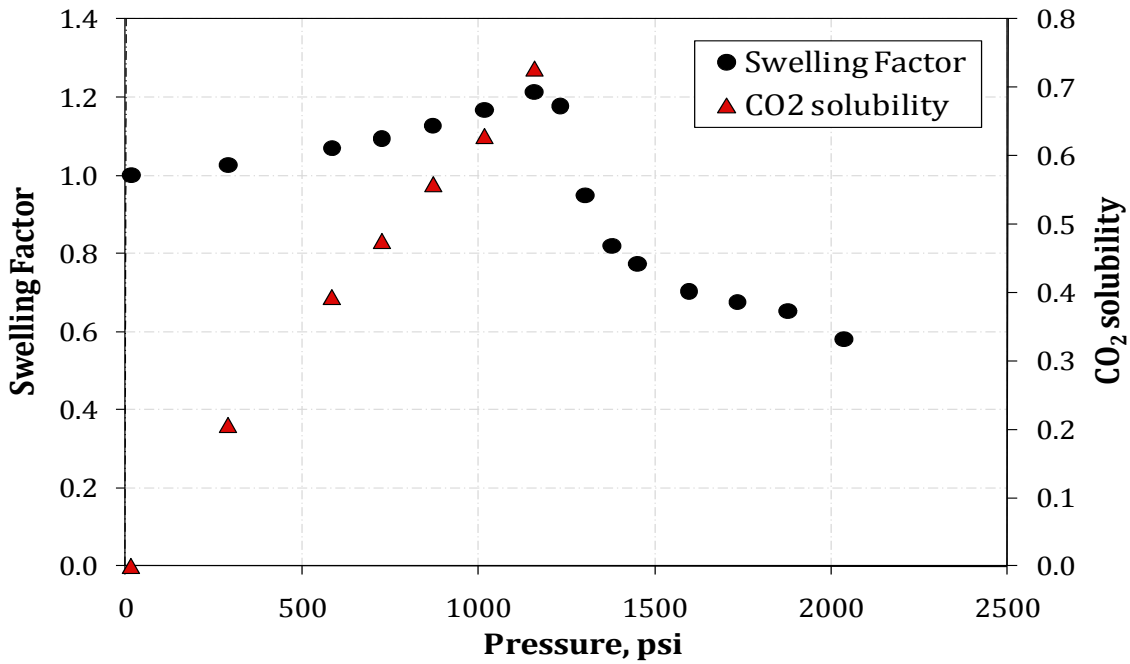

Figure 11 Effect of pressure on CO_2 solubility and swelling factor at 110°F

Effect of System Temperature

Swelling/extraction experiments were performed under various temperatures from 105°F to 125°F. Effects of temperature on CO_2 solubility and oil swelling/extraction curve are shown in Figure 12 and Figure 13. CO_2 solubility increased with increasing pressure and decreased with increasing temperature. The rate of oil swelling decreased with increasing temperature. The pressure at which oil swelling reached maximum or at which CO_2 began extracting components from crude oil increased with increasing temperature, ranging from 1159 psi to 1260 psi at a temperature range of 105°F to 125°F. The rate of oil shrinkage decreased with increasing temperature.

The ability of CO_2 to extract hydrocarbon from the crude oil depends on its density. At higher temperature, a higher pressure results in a density equivalent to its density at a lower temperature. Holm and Josendal report that the extraction of liquid hydrocarbons into CO_2-rich vapor phase occurs when the density of CO_2 is at least 0.25 to 0.35 gm/cc. The extraction of oil starts at density of CO_2, 0.26 gm/cc at 105 ºF and 1150 psig. At 125 ºF, the pressure of CO_2

needs to increase to have an equivalent density to start the extraction and it is in the neighborhood of 1300 psia.

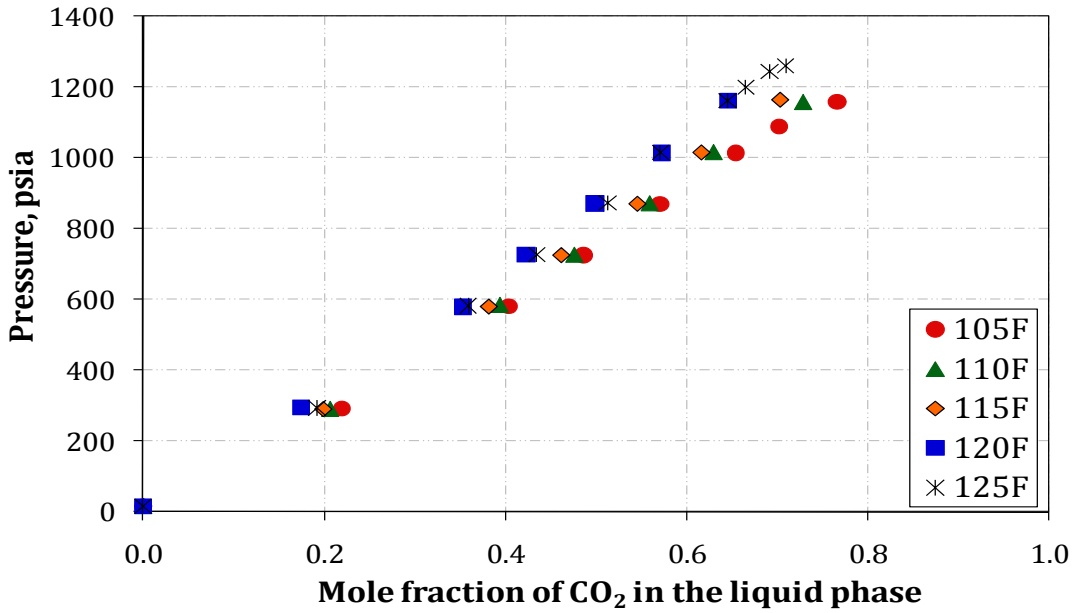

Figure 12 Effect of temperature on CO_2 solubility

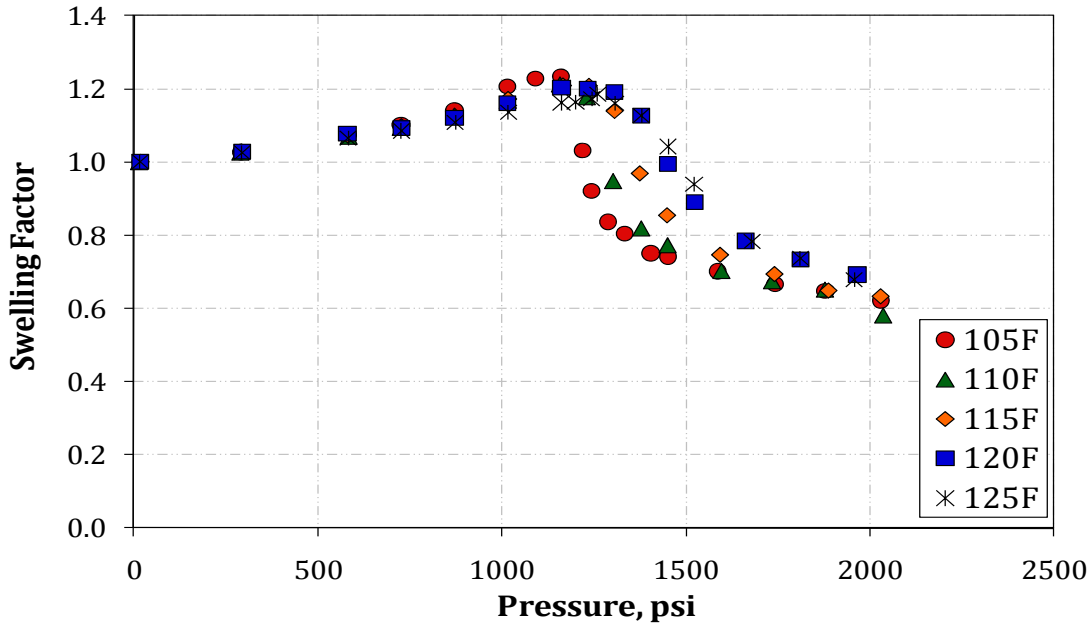

Figure 13 Effect of temperature on Swelling/ Extraction curves

Viscosity Measurements

A Cambridge Applied Systems' high pressure viscometer (ViscoPro 2000 System 4-SPL-440 with Viscolab software) utilizes an electromagnetic concept to measure viscosity of pure crude oil and/or crude oil/CO_2 mixture. The accuracy of this viscometer was validated earlier by Ahosseini *et al.* (2008), first by using standard calibration solutions, then by comparing viscosity values of n-hexane measured using this viscometer with literature values.

Principle of Operation

The viscometer utilizes the principles of annular flow around an axially oscillating piston. It contains two magnetic coils inside a stainless steel body. A low mass stainless steel piston inside the measurement chamber is magnetically forced back and forth in the fluid. As the piston is pulled toward the bottom of the measurement chamber, it forces the fluid at the bottom of the chamber to flow around the piston toward the sensor opening where it interchanges with the normal flow of the fluid. On the upward piston stroke, fresh process fluid is pulled around the piston to the bottom of the measurement chamber. The time required for the piston to move a fixed distance is related to the viscosity of the fluid in the chamber. Temperature is measured continuously with the use of a platinum Resistance Temperature Detector (RTD) mounted at the base of the measurement chamber.

Experimental Setup and Specifications

The schematic of the setup is shown in Figure 14 along with its image in Figure 15. The high pressure sensor is placed inside a temperature-controlled oven and connected to a manual high pressure syringe pump (Model No. 50-575-30; 30,000 psi). The sensor is capable of measurements from 0.2 to 10,000 cp at a maximum pressure of 137.9 MPa and in a temperature range of 233.15K to 463.15K .The measurement chamber of the high pressure sensor is connected to a rupture disk (RD) and a precision pressure transducer (PT). When the setup is used for viscosity measurements of pure crude oil as a function of pressure, a high-pressure generator is required. When it is used for viscosity measurements of crude oil/CO_2 mixture, the pressure of the system is increased by CO_2 injection. ISCO 260D pump- Model 1020 BBB-4 is used for CO_2 transfer/injection. A view cell placed inside the oven allows observations of crude oil/CO_2 interaction. During pressurization process, the time required for the contents in the system to equilibrate under a particular pressure and temperature is minimized by a circulation pump-Micropump, Inc. Model 415A.

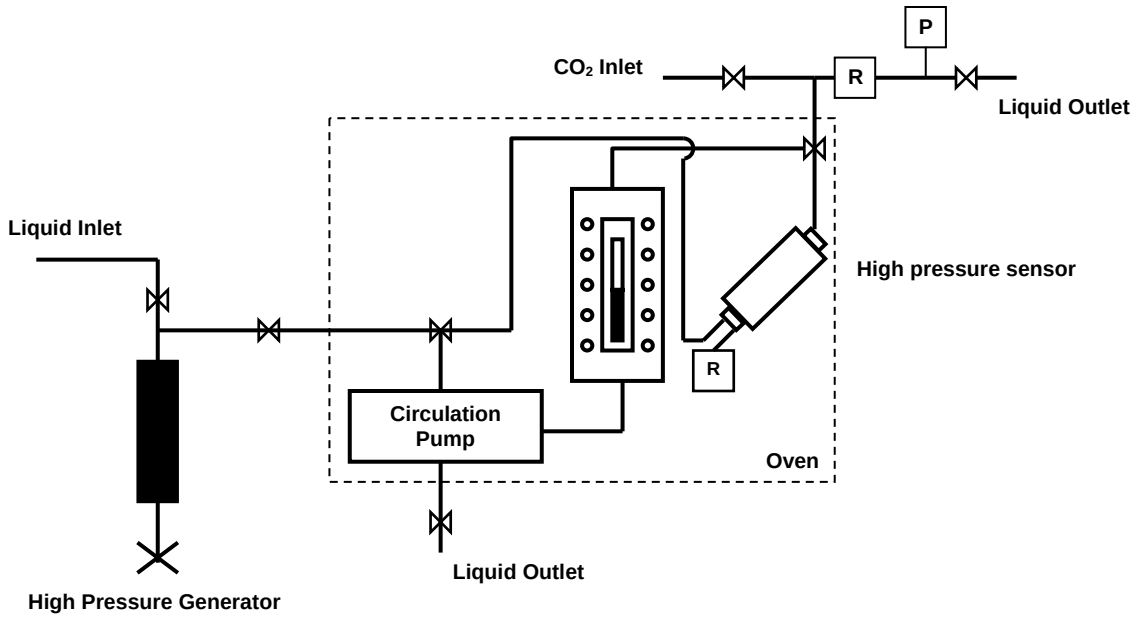

Figure 14 Schematic of high-pressure viscosity measurement setup

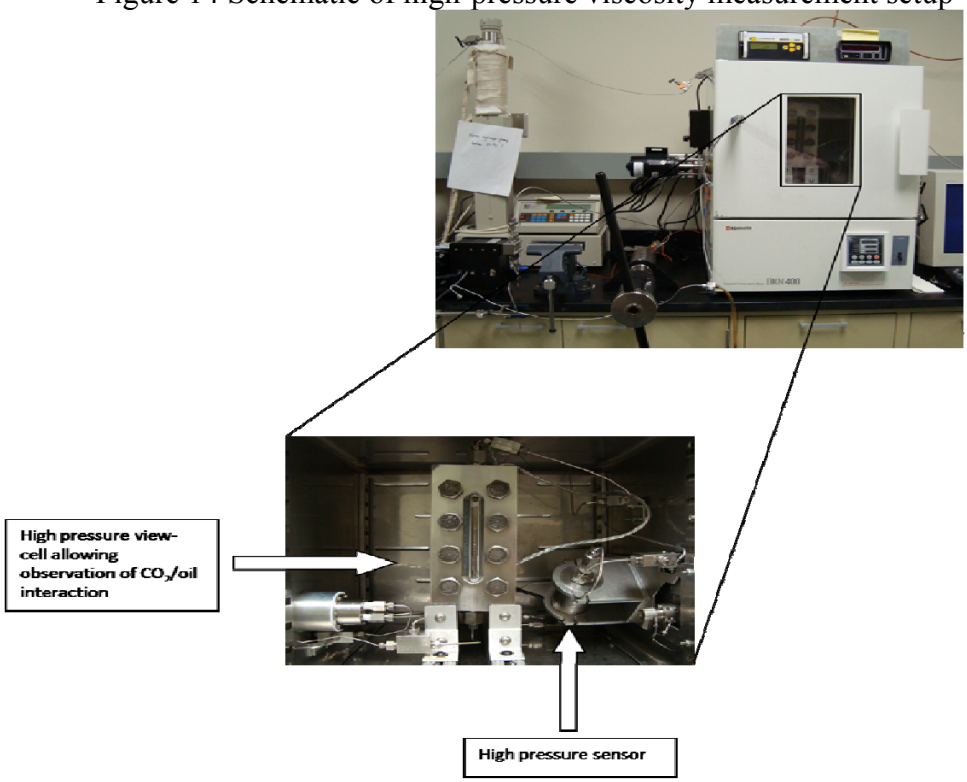

Figure 15 Image of the high-pressure viscosity measurement setup

Oil Viscosity Measurement Procedure

The schematic in Figure 16 illustrates a basic layout for using a high pressure generator. A reservoir (R) is shown connected by means of valves and fittings to a component (C) that is to be pressurized. With valve "B" closed and valve "A" open, the handle of the high pressure generator is rotated counter-clockwise to create enough space inside the cylinder body to store the crude oil. Valve "A" is then closed and valve "B" is opened. By rotating the high pressure generator handle clockwise slowly, the piston will compress the fluid to develop pressure in the component that is to be pressurized. If sufficient pressure is not reached in one stroke, the system can be "recycled." Valve "B" can be closed in order to maintain pressure in the components. Valve "A" is then opened, and fluid is again drawn into the Pressure Generator from the reservoir. Closing Valve "A" and opening Valve "B" will now allow the Pressure Generator to be operated to develop increased pressure in the component.

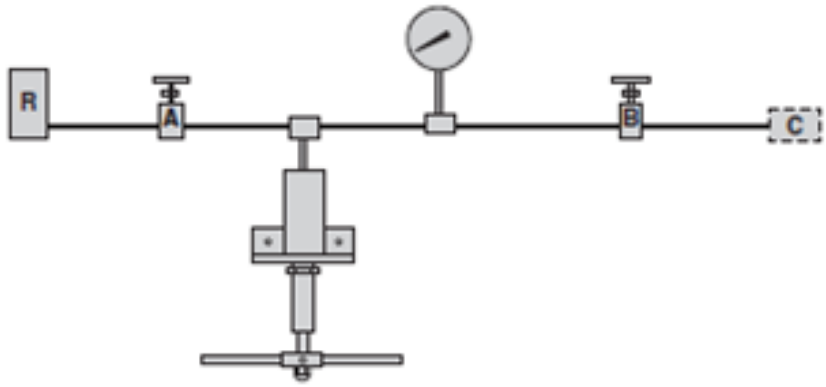

Figure 16 High pressure generator

In this experimental setup, the oil was pumped into the cylinder body using the manual high pressure syringe pump until the cylinder body is full. Excessive fluid introduction would cause pressure buildup in the cylinder body; therefore, the system outlet must have been opened before Valve "B" was opened to avoid damaging the sensor. The oil was introduced into the system and into the measurement chamber, opening both Valve "A" and Valve "B" and bypassing the high pressure generator. Temperature of the oven was set at the desired temperature. When the system was at thermal equilibrium, the system was purged to dislodge any potential bubbles. Temperature reading was taken from the RTD of the viscometer. Valve "A" was closed, Valve "B" was opened when the system was pressurized. The viscometer also

needed to be turned off. By rotating the handle of the high pressure generator slowly clockwise, pressure was developed in the system until a desired pressure had reached. Viscosity reading was taken when temperature and pressure of the system is stable.

Oil/CO_2 Mixture Viscosity Measurement Procedure

Temperature of the oven was set constant at the desired temperature. Temperature of ISCO pump was set constant at the desired temperature. Pressure of the pump was set constant at the maximum anticipated pressure. Liquid was introduced into the measurement chamber and into the view cell. When the system was at thermal equilibrium, the system was purged to dislodge any potential bubbles. Temperature reading was taken from the RTD of the viscometer. Viscometer needed to be turned off when CO_2 was introduced into the system. The system pressure was increased in discrete steps by CO_2 injection from the top of the view cell. CO_2 injection was stopped when a desired pressure was achieved. During pressurization process, a micropump was used to circulate the liquid inside the system to help accelerating the mass transfer of the gas phase into the liquid phase. Reading was taken when temperature and pressure of the system were stabilized.

Results and Discussions

Figure 17 shows the relationship of viscosity of pure crude oil with pressure at 110°F. Figure 18 demonstrates the effect of CO_2 dissolution into crude oil on viscosity of crude oil at 110°F. As a result of CO_2 dissolution into the liquid phase, viscosity of the liquid phase was reduced. At pressures above 1000 psig, the effect of CO_2 on oil viscosity is minimal. The viscosity of the liquid phase was reduced as much as a factor of five in the near miscible region, from 1100 psig to 1350 psig.

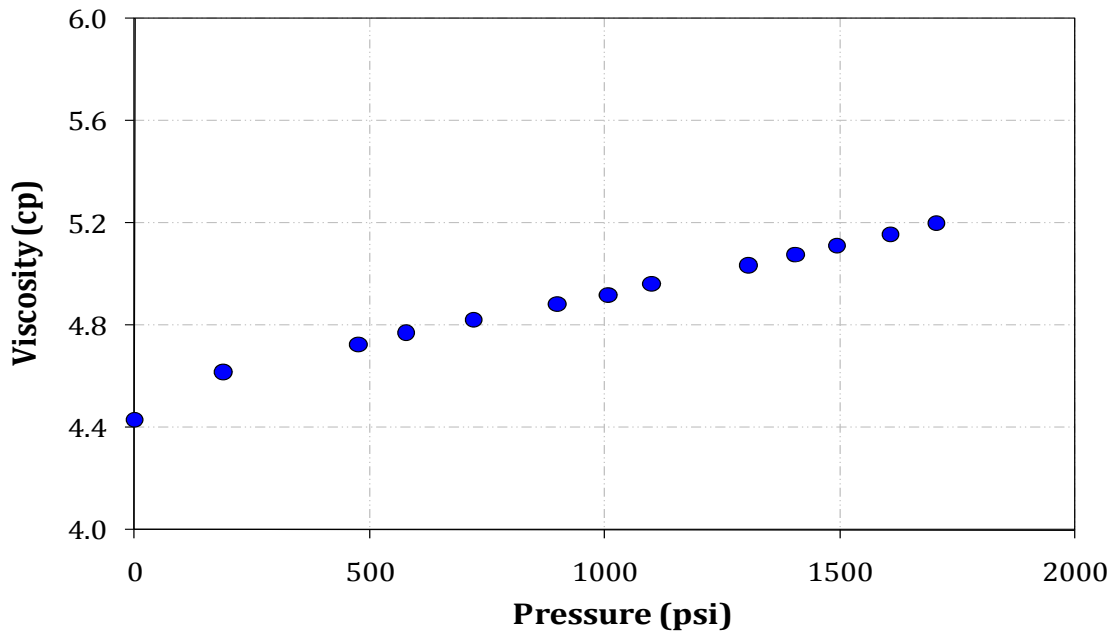

Figure 17 Effect of pressure on Ogallah oil viscosity at 110°F

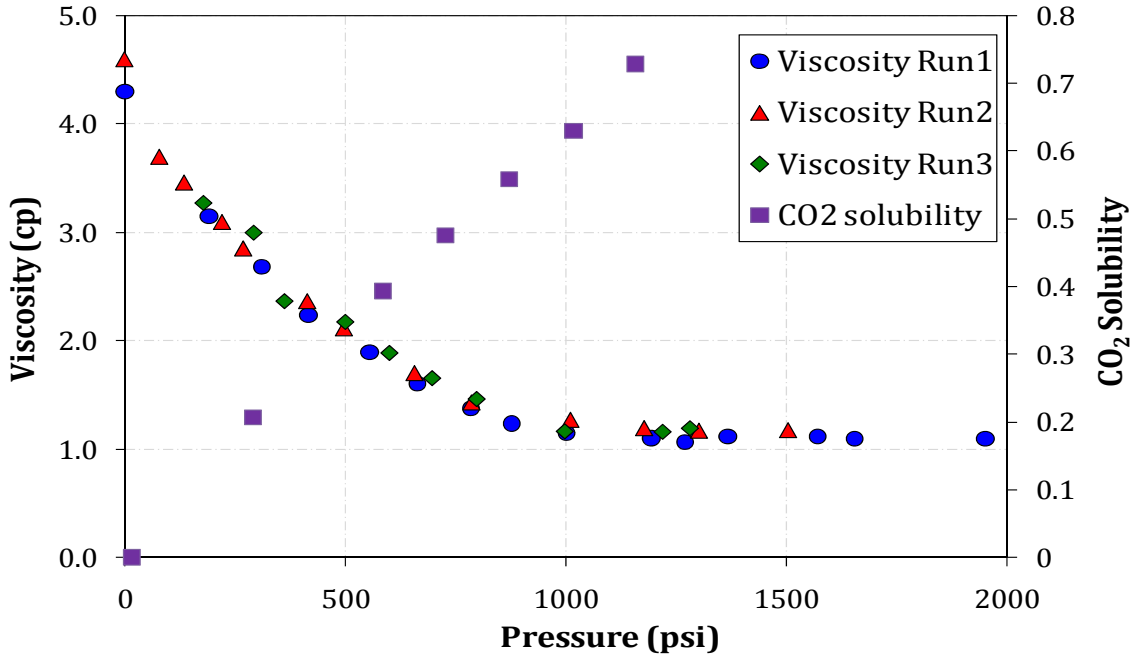

Figure 18 Viscosity of crude oil saturated with CO_2 at 110°F

Estimation of MMP

The relationship between the phase behavior observed in swelling/extraction tests and MMP measured by slim-tube experiment has been investigated by several researchers. Harmon

and Grigg (1988) reported a relationship between the pressure required to initiate significant extraction in swelling/extraction tests and the MMP from slim-tube experiment. They proposed that a rapid rise in CO_2 upper-phase density of measurement due to the extraction of hydrocarbon components from the crude oil corresponds to the process by which multiple-contact miscibility is developed. However, Hand and Plnczewski (1990) concluded no such direct relationship between the two tests because the vapor phase density, dominated by high solvent CO_2 concentration, is not a sensitive indicator of the onset of major extraction, or of MMP. In this work, we observed MMP can be graphically derived from the extraction test. By examining the extraction test results with MMP measured from the slim-tube experiment, a relationship exists between these two tests if the initial oil volume tested in view cell is small (12%) and the relative volume of oil due to extraction falls below 0.8 over the pressure range investigated. Figure 19 present swelling/extraction test curves of oil/CO_2 system at 110 ºF and 125 ºF. The rate of slope changes in two distinct stages in each of the two extraction curves. Drawing lines through the major extraction and secondary stages, the pressure at the intersection of these two lines is close to MMP determined with the slim-tube experiment. As shown in this figure, the pressures at the intersection point are 1340 psig and 1640 psig at 110 ºF and 125 ºF, respectively. The MMP determined from slim-tube for oil B/CO_2 were 1350 psig and 1650 psig.

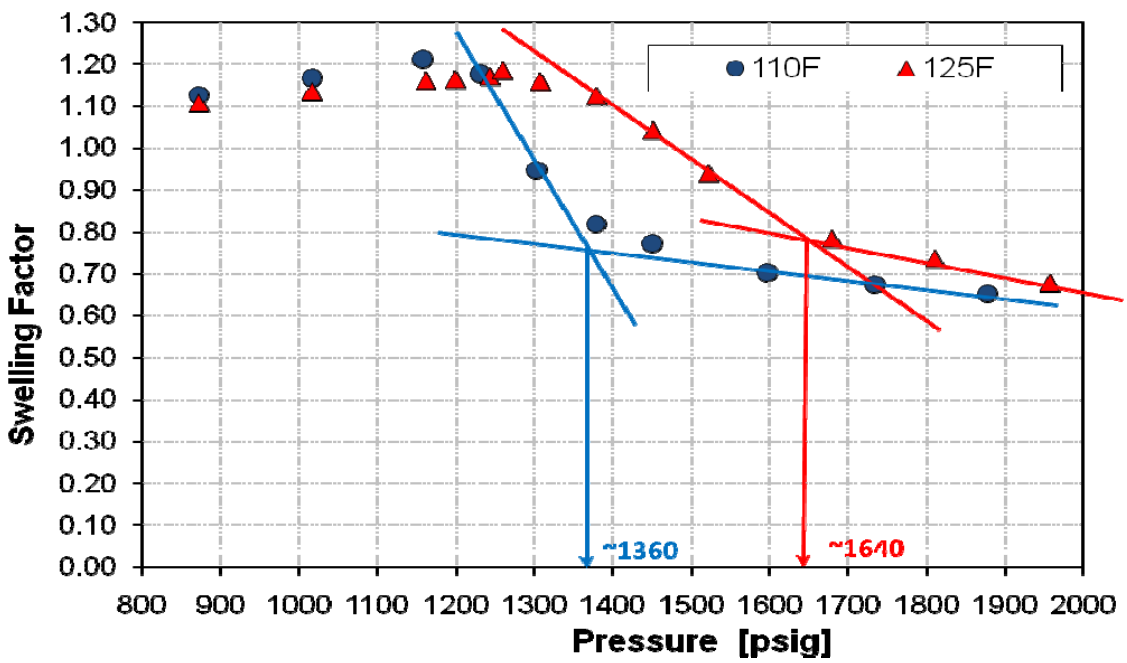

Figure 19 Estimation of MMP from extraction test of Ogallah crude oil

Summary

1) CO_2 solubility increases with increasing pressure and decreases with increasing temperature. As a result of CO_2 dissolution into the liquid phase, the liquid phase swells. The degree of swelling depends on pressure and temperature.
2) The pressure at which CO_2 begins to extract significant amounts of hydrocarbons from crude oil increases with increasing temperature. The amount of extraction increases with increasing vapor-phase volume (decreasing initial oil volume) and decreases with increasing temperature.
3) Significant extraction started at pressure of 1150 psig & 110°F. Extraction or vaporization of hydrocarbons into the CO_2 rich phase is the primary mechanism for oil recovery in the near-miscible region, from 1100 psig to 1350 psig & at 110°F
4) Swelling/extraction tests provide valuable phase behavior data which is used later to tune the phase behavior model.
5) A nearly five-fold reduction in oil viscosity was achieved in the near-miscible region with CO_2 injection.
6) The reduction of oil viscosity improved the total mobility ratio between reservoir oil and the displacing fluid, which will affect the recovery efficiency in a favorable way.
7) Viscosity measurements are useful in tuning the phase behavior model.
8) The MMP estimated by the swelling/extraction test graphically is close to what determined from the slim-tube experiment.

4. Task 4.3 Phase Behavior Model

A phase behavior model based on the Peng-Robinson equation of state was used to characterize the phase behavior interaction between CO_2 and oil. The model was adjusted to match the saturation pressure and swelling factors derived from the swelling tests. This phase behavior model was used in a compositional reservoir simulator GEM (from Computer Modeling Group, Inc.) to match slim-tube experiments. Parameters in the model were adjusted accordingly to obtain the best match. The final tuned simulator model was used as the basis for describing core flood tests and extended simulations for potential field applications.

Equation of State

Equations of State (EOS) have been introduced widely to model and predict CO_2-crude oil phase behavior. An EOS is an algebraic relationship between pressure, temperature, and molar volume for a single component or a mixture. Peng-Robinson EOS was used in this study to describe the fluid properties and the oil/CO_2 interaction.

$$p = \frac{RT}{v-b} - \frac{a}{v^2 + 2vb - b^2}$$

The parameters a and b are defined using the following mixing rule for mixtures,

$$a = \sum_i x_i S_i$$

$$S_i = \sqrt{a_i} \sum_j x_j \left(1 - d_{ij}\right) \sqrt{a_j}$$

$$b = \sum_i x_i b_i$$

Where, d_{ij} is an empirically determined interaction coefficient.

For pure components, the parameter a_i and b_i are expressed in terms of the critical properties and the accentric factor:

$$\sqrt{a} = \sqrt{a_c \alpha}$$

$$\sqrt{a_c} = \sqrt{\Omega_a} \left(RT_c\right) / \sqrt{p_c}$$

$$\sqrt{\alpha} = 1 + \kappa \left(1 - \sqrt{T / T_c}\right)$$

$$b = \Omega_b RT_c / p_c$$

Where, Ωa and Ωb are the EOS parameters with the default values of 0.45723553 and 0.077796074 for the PR EOS.

The κ is obtained from the following empirical correlations,

$$\kappa = 0.379642 + 1.48503\omega - 0.164423\omega^2 + 0.016666\omega^3$$

While the application of the EOS to simple mixtures is relatively straightforward, crude oil systems pose many seemingly insurmountable problems. The essential infinite number of components contained in a typical crude oil makes it impossible to obtain a complete chemical analysis. Standard oil analysis lumps all components heavier than C36 into a single C36+ pseudo-component characterized by its average molecular weight and density. Therefore, the parameters of the EOS were adjusted so that the EOS could reproduce the laboratory-determined oil properties and the observed oil/CO_2 interaction.

Slim tube model was constructed using 1-D compositional simulator with the tuned EOS. Simulated slim tube results were compared with experimental slim tube results. The following sections describe in detail the development of phase behavior model/slim tube model in CMG^{TM} software and the application of this phase behavior model to match with experimental PVT data and slim tube results.

Phase Behavior Modeling Using WINPROP

WinProp, a CMG software was utilized to build the phase behavior model. The EOS requires the following properties for each component, critical pressure (Pc), critical temperature (Tc), acentric factor (ω), and interaction coefficients between different components (d_{ij}) to perform phase equilibrium calculations. The molecular weight (MW) is also required to calculate mass densities. Additional factors such as the volume shifts τ, and the equation-of-state parameters Ωa and Ωb can also be adjusted for each component to enhance the equation of state predictions.

Pure hydrocarbon components were selected from the software library list, as well as generalized single carbon number (SCN) petroleum fractions FC6 through FC45. The specific gravities, molecular weights and boiling points of the SCN fractions were obtained from Whitson (1983). The critical properties of these fractions were calculated with the Lee-Kesler correlation. The heavy lumped component C36+ was defined using specific gravity and molecular weight. Physical and critical properties of C36+ were assigned using Twu and Lee-Kesler correlation respectively. For accentric factors, the Lee-Kesler correlation was recommended for petroleum fractions. Equilibrium phase viscosities were calculated with the Pedersen viscosity corresponding states model. The Pedersen viscosity correlation uses the principle of corresponding states to calculate the viscosity of a component or mixture, knowing the viscosity

of a reference substance at the same conditions of reduced pressure and temperature. The deviation from simple corresponding states is accounted for by a "rotational coupling coefficient", α. The reference substance for the Pedersen model is methane. The viscosity of the mixture is calculated according to the following formula:

$$\frac{\mu_{mix}(P,T)}{\mu_o\,(P_o,T_o)} = \frac{T_{c,mix}}{T_{c,o}}^{-1/6} \frac{P_{c,mix}}{P_{c,o}}^{2/3} \frac{MW_{mix}}{MW_o}^{1/2} \frac{\alpha_{mix}}{\alpha_o}$$

When the components representing the fluid model had been selected and their compositions had been specified, a grouping scheme was performed primarily for the purpose of speeding up the simulation running time. Whitson suggested that C7+ should be grouped into NH pseudo-components given by,

$$N_H = 1 + 3.3\log(N-7)$$

The groups are separated by molecular weights MI given by,

$$M_I = M_{C_7}\left(M_N / M_{C_7}\right)^{I/N_H}$$

where N = CN of the heaviest fraction in the fluid description and I = 1 to NH

Therefore,

NH = 5 pseudo-groups

Group 1 < M1 = 138.303

M1 <Group 2 < M2 = 191.276

M2 < Group 3 < M3 = 264.539

M3 < Group 4 < M4 = 365.865

Finally an 8-component EOS fluid model was obtained after grouping the components as

Group 1: C3 + iC4 + nC4

Group 2: nC5+ iC5

Group 3: C6

Group 4: C7 – C9

Group 5: C10 – C13

Group 6: C14 – C18

Group 7: C19 – C25

Group 8: C26 – C36+

Equation of State Characterization

Figure 20 and Figure 21 present the experimental data and the simulated data after tuning EOS parameters. Molecular weight (MW) of the heavy fraction was adjusted to match the oil density. Coefficients of Pedersen viscosity correlation were adjusted to match the oil viscosity. Binary interaction coefficients (BIC) between CO_2 and the hydrocarbon components as well as CO_2 volume shift factor were adjusted to match saturation pressure and swelling data. Table 4 shows the adjustment of each parameter to achieve the match.

Table 4 Adjustments of EOS parameters

Variable	**Lower Bound**	**Upper Bound**	**Initial Value**	**Final Value**
MW C26 to C36+	5.07E+02	7.60E+02	6.34E+02	5.98E+02
Volume shift of CO_2	-1.54E-01	9.20E-01	0.00E+00	9.11E-01
BIC (C7-C9)-CO_2	0.00E+00	2.00E-01	1.50E-01	0.00E+00
BIC (C10-C13)- CO_2	0.00E+00	2.00E-01	1.50E-01	0.00E+00
Coefficient of viscosity correlation # 4	1.00E+00	2.22E+00	1.85E+00	1.04E+00
Coefficient of viscosity correlation # 5	4.14E-01	6.21E-01	5.17E-01	6.21E-01

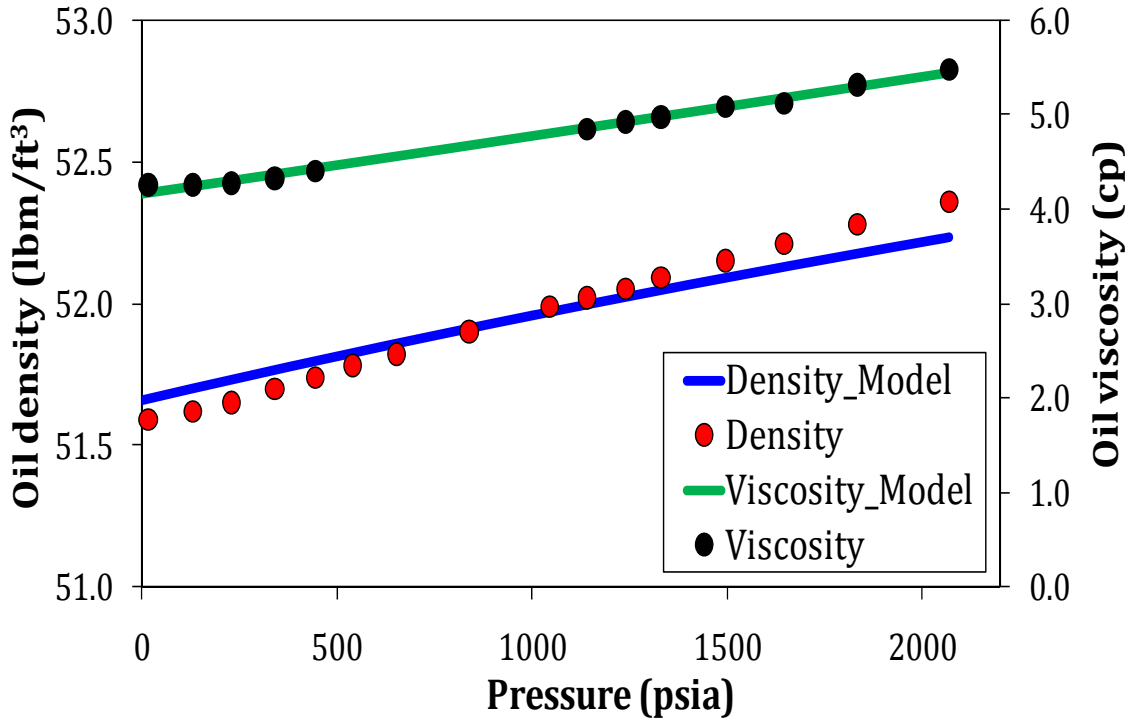

Figure 20 Comparison of viscosity/density experimental data and simulated data

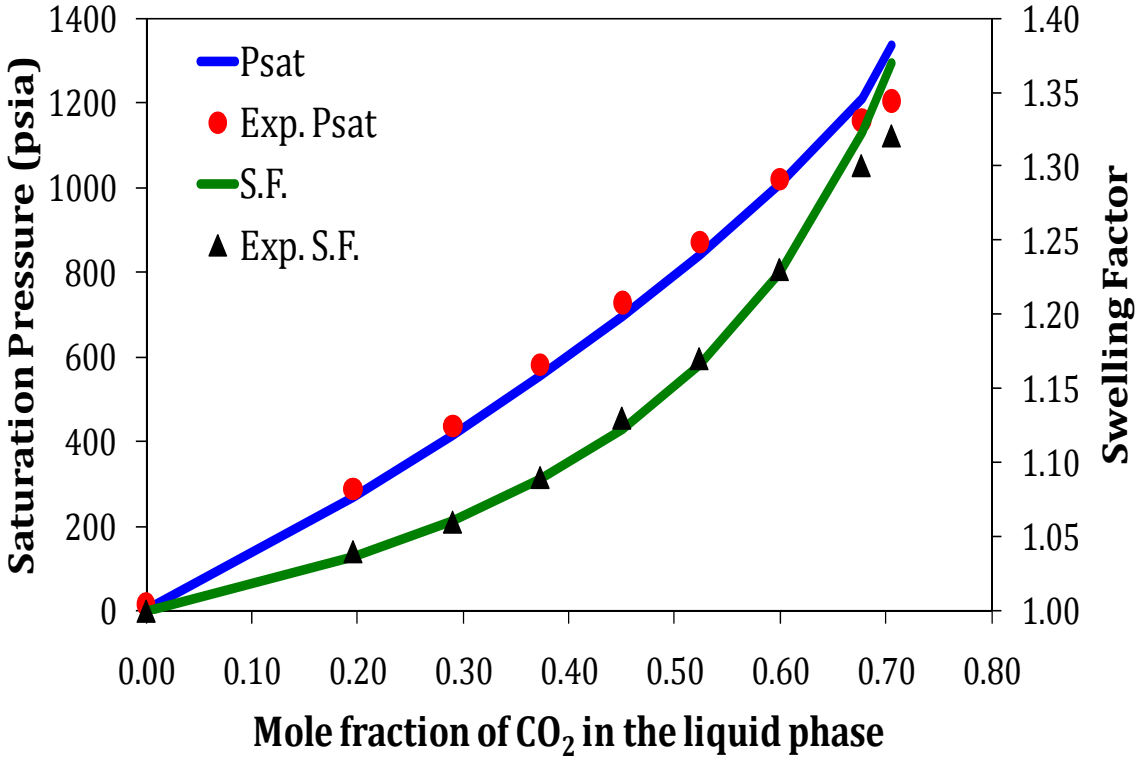

Figure 21 Comparison of saturation pressure/swelling factor experimental and simulated data

The maximum percentage error between simulated data and experimental data after tuning the EOS is presented in Table 5.

Table 5 Maximum percentage errors between simulated and experimental data

	Maximum error percentage
Viscosity	3 %
Density	1 %
Saturation pressure	7 %
Swelling factor	1 %

Slim Tube Experiment Modeling Using GEM

A slim tube model was created in compositional model simulator of GEM from CMG package with the phase behavior model derived from this phase behavior study. The slim tube was represented by a one dimensional linear model using 320 grid blocks. The grid block sizes were 0.125 ft, 0.0185 ft and 0.0185 ft in I, J, K direction respectively. One injector and one producer were incorporated at the ends of the model. Some relevant information of slim tube model is summarized in Table 6.

Table 6 Slim tube model properties

Length, ft	40
Porosity, PV	0.367
Permeability, mD	4900
Pore Volume, cc	142.3
No. of blocks	320
Grid size in I direction, ft	0.125
Cross section, ft^2	0.0003423
Grid size in J and K direction, ft	0.0185
Geometry	Square Cross-section

The slim tube gas/oil relative permeability data used in this model were obtained from Negahban and Kremesec (1992). A number of slim tube displacements were simulated. Figure

22 compares the recovery efficiency from simulation and experimental work at 1.2 PV of CO_2 injected. As shown by Figure 22, the phase behavior model predicts the MMP and the oil recovery reasonably well.

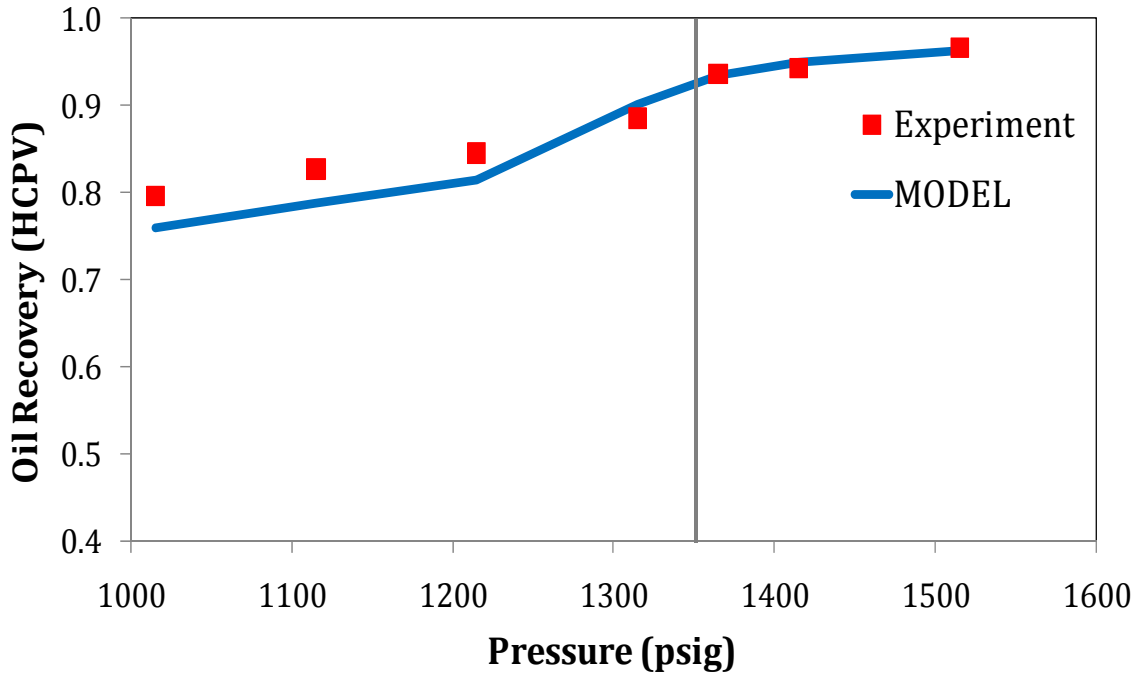

Figure 22 Comparison of simulated MMP and experimental MMP

Summary

1) A phase behavior model based on the Peng-Robinson equation of state was used to characterize the phase behavior interaction between CO_2 and oil.
2) The parameters were adjusted to match the saturation pressure and swelling factors derived from the swelling tests.
3) The phase behavior model successfully modeled the measurement of MMP from the slim-tube experiment. This 8 pseudo-component of hydrocarbon phase behavior model was further reduced to one with 4 pseudo-components and used in compositional reservoir model to simulate CO_2 injection process.

5. Task 4.4 Flow Tests with Core Samples at Near Miscible Conditions

Arbuckle reservoir rock and two queried rock samples, Berea sandstone and Baker dolomite containing Arbuckle crude oil at waterflood residual oil saturation were flooded with CO_2 to determine the residual oil saturation to CO_2. A series of displacement experiments were conducted in which the pressure is systematically varied at near miscible conditions. The residual oil saturation remaining in the core sample at the end of each experiment was evaluated.

Completion of this task allowed us to examine the effect of water saturation, and mobility ratio on oil recovery at near miscible conditions. The core flooding experimental results was used in developing a representative flow model to simulate near miscible displacement physics in reservoir rocks.

Cores from Arbuckle reservoirs are limited. Core tests were made using Berea sandstone, Baker dolomite and Arbuckle dolomite. Berea sandstone and Baker dolomite were quarried rock samples whereas Arbuckle dolomite was cored sample from Hadley well, Bemis-Shutts Field at Ellis County, Kansas. Before cores were epoxy encased and cast inside an aluminum cylinder with high strength epoxy, at least three measurements of the diameter and the length of each core were obtained. The average value of the diameter and the length was used to calculate the area and the bulk volume of each core. The dry weight of the core holder was recorded.

Upon completion of each core flow test, the cores were cleaned to restore to its initial condition and reused for the next experiment. The core cleaning procedure is outlined as follows:

1) The cores were successively cleaned with methylene chloride and methanol. At least 10 PV of methylene chloride followed by 10 PV of methanol was injected. The sequence was repeated at least three times until the effluent was clear.
2) The cores were blown dry by CO_2 and vacuumed to remove residual air/CO_2.
3) The cores were fully saturated with either brine or crude oil, depending on which type of core flow tests would be conducted. Brine was used for tertiary CO_2 floods. Crude oil was used for secondary CO_2 floods.

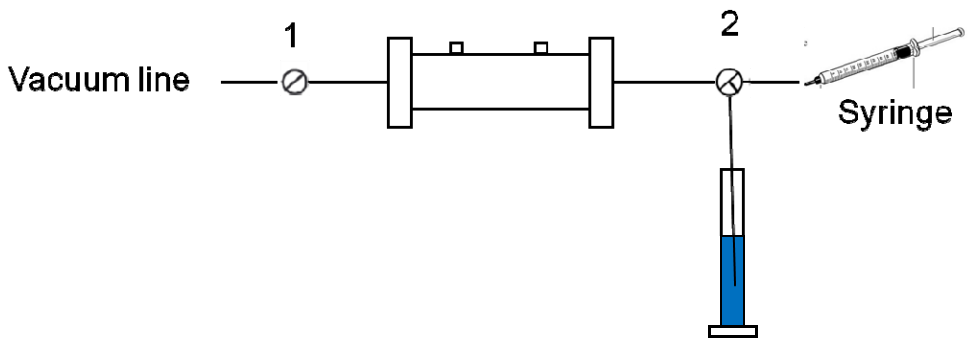

Figure 23 Vacuum and saturation setup

Figure 23 shows the experimental setup for vacuuming and saturating the cores. The procedures to vacuum and saturate the core with brine are described as follows,

1. VACUUM (700mmHg): Open Valve 1, Close Valve 2
2. DRY WEIGHT MEASUREMENT: Close Valve 1 & 2, Disconnect the core holder with the vacuum line, Weigh the core holder with all the fittings (Weight of all the fitting would be subtracted later)
3. The purpose of the syringe was to ensure that the line which immersed in the graduated cylinder was clear of air.
4. SATURATION: Close Valve 1, Open Valve 2 (Brine will be drawn in the core holder), Wait until the level of the brine did not change (During the saturation process, the line was always ensured to be immersed in the brine)
5. PORE VOLUME ESTIMATION: Estimate the change of volume of brine in the graduated cylinder before and after brine was suck into the evacuated cores (dead volume from fittings must be subtracted).

Brine with 1wt% total dissolved solids (TDS) was used. Composition of brine was 0.5 wt% $MgCl_2$ and 0.5 wt% $CaCl_2$ in deionized water. Brine was filtered using 0.22 micron membrane (Micron Separations Inc.) before use. Density of brine was obtained using the densitometer. Viscosity of brine was measured using Brookfield DV-III Ultra programmable rheometer. Density and viscosity of brine are summarized in Table 7.

Table 7 Density/Viscosity of Brine at 86°F/110°F

	T = 86°F	T = 110°F
Brine density, g/cc	1.0007	0.9959
Brine viscosity, cp	0.8350	0.7250

Characterization of Core Samples

Core characterization includes determining pore volume, porosity and permeability for each core. The pore volume was approximated by the change of volume of brine in the graduated cylinder before and after brine was drawn into the evacuated cores. Pore volume of each core, however, can be determined more accurately by two ways, gravimetric method and tracer tests. In the gravimetric method, the pore volume of each core was computed based on the weight difference of the core before and after brine was imbibed into the dry and evacuated core. In the tracer tests, concentration of tracer solution is analyzed; equal area technique is utilized to calculate pore volume of each core. Both techniques are discussed in detail in the following sections.

Gravimetric Method

The core holder was weighed before and after fully saturated with brine. Pore volume of each core was calculated as follows:

$$PV = \frac{W_s - W_d}{\rho}$$

Where,

PV = pore volume (cc)

W_s = weight of the core holder when it is 100% saturated with brine (g)

W_d = weight of the core holder when it is dry (g)

ρ = density of brine at the testing temperature (g/cc)

Core porosities were calculated as follows:

$$\phi = \frac{PV}{BV}$$

Where,

Φ= porosity

PV = pore volume (cc)

BV = bulk volume (cc)

Tracer Tests

Tracer tests were performed to confirm the pore volume of a core. A tracer is an injected substance that is both measurable (e.g. through UV-visible detection) and conserved (i.e. not

retained, destroyed or created by the core). 1 wt% $MgNO_3$ was used as a tracer in this study. If tracer concentration is recorded at the core outlet and plotted as a function of time, an S-shaped curve will form. The S-shaped curve is caused by dispersion of one fluid into another; otherwise, there would be an instantaneous change in tracer concentration at breakthrough. Tracer data is typically normalized to scale the tracer concentration values from zero to one. A typical normalized tracer curve is shown in Figure 24.

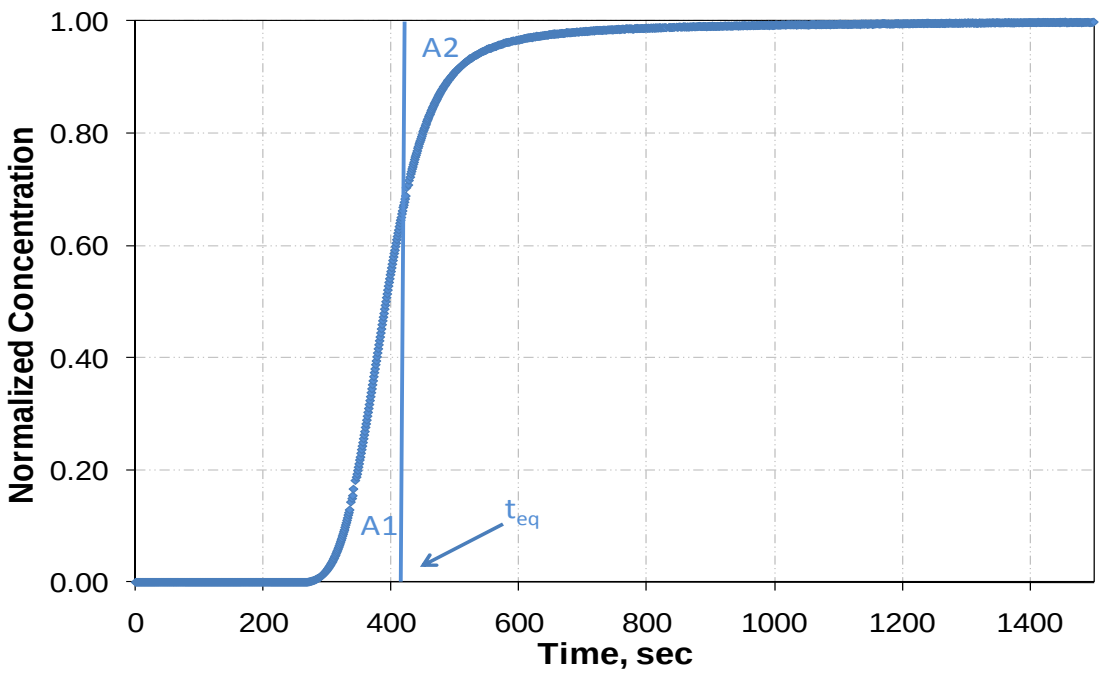

Figure 24 Estimation of pore volume from tracer tests

Normalized concentration is calculated as follows:

$$C_B = \frac{C_B^* - C_{Bo}}{C_{Bi} - C_{Bo}}$$

Where,

C_B = normalized tracer concentration

C_B*= measured tracer concentration

C_{Bo}= initial concentration of brine

C_{Bi} = maximum tracer concentration

Equal-area technique is utilized to compute PV of a core as follows:

$$PV = \left(\left(t_{eq} - t_o\right) \times q\right) - V_d$$

Where,

V_d = any dead volume (cc)

q = tracer flowrate (cc/min)

t_o = time at which tracer injection starts (min)

t_{eq}= time at which equal area under each side of the curve reaches, A1 = A2

Areas on each side of the tracer concentration, A1 & A2, were calculated using trapezoidal rule. t_{eq} is at A1 = A2.

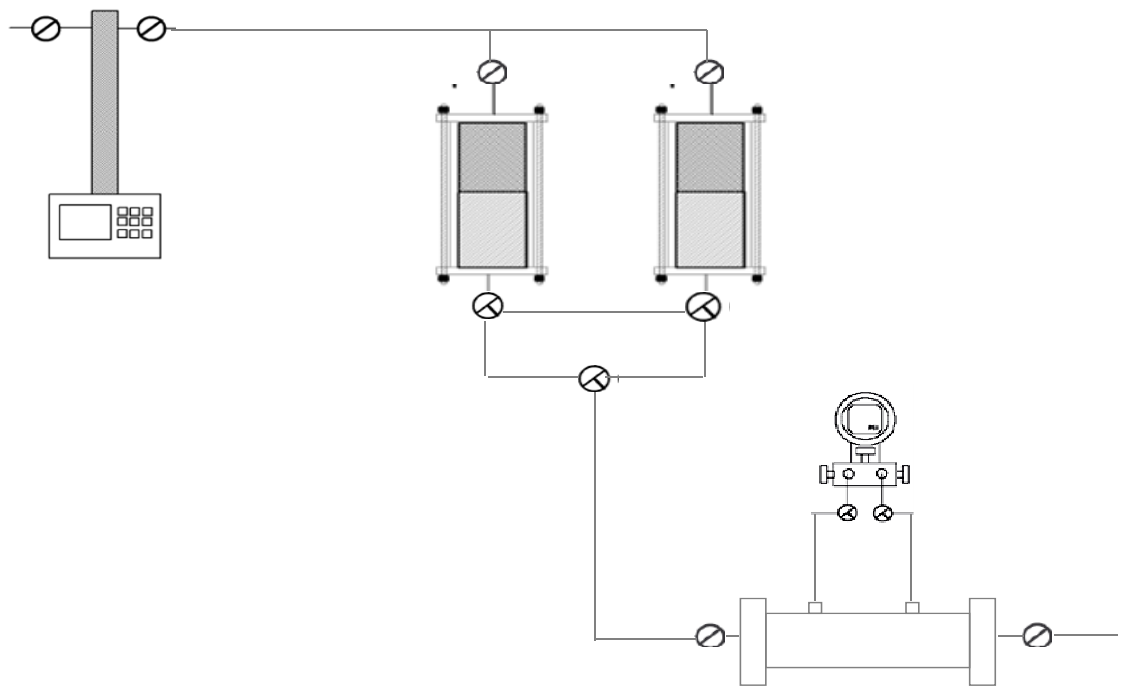

Figure 25 Schematic of tracer test setup

Figure 25 shows the schematic of the tracer setup. The injection system consists of an ISCO, Inc. 260DM syringe pump (for mineral oil transfer and injection) and two transfer cylinders (for tracer solution/brine/mineral oil storage). 1 wt% $MgNO_3$ was used as a tracer. The inlet of the core holder is connected to the injection system. The three-way valve allows switching the flow between tracer solution and brine. The outlet of the core is connected to an UV-visible detector. The UV-visible detector should be turned on and set at a wavelength of 302 nm at least an hour prior tracer tests. The flow cell of the detector should be cleaned by methylene chloride, followed by acetone and finally brine injection.

Brine passed through core at a constant flow rate until UV-visible detector read a steady concentration value. At this point, the detector was zeroed and the three-way valve was switched to tracer injection. The switchover time needed to be recorded manually.

When tracer concentration did not change over time, the valve was switched back to non-tracer injection to displace the tracer solution from the core. Again, the switchover time needed to be recorded manually.

Core Floods Experimental Setup

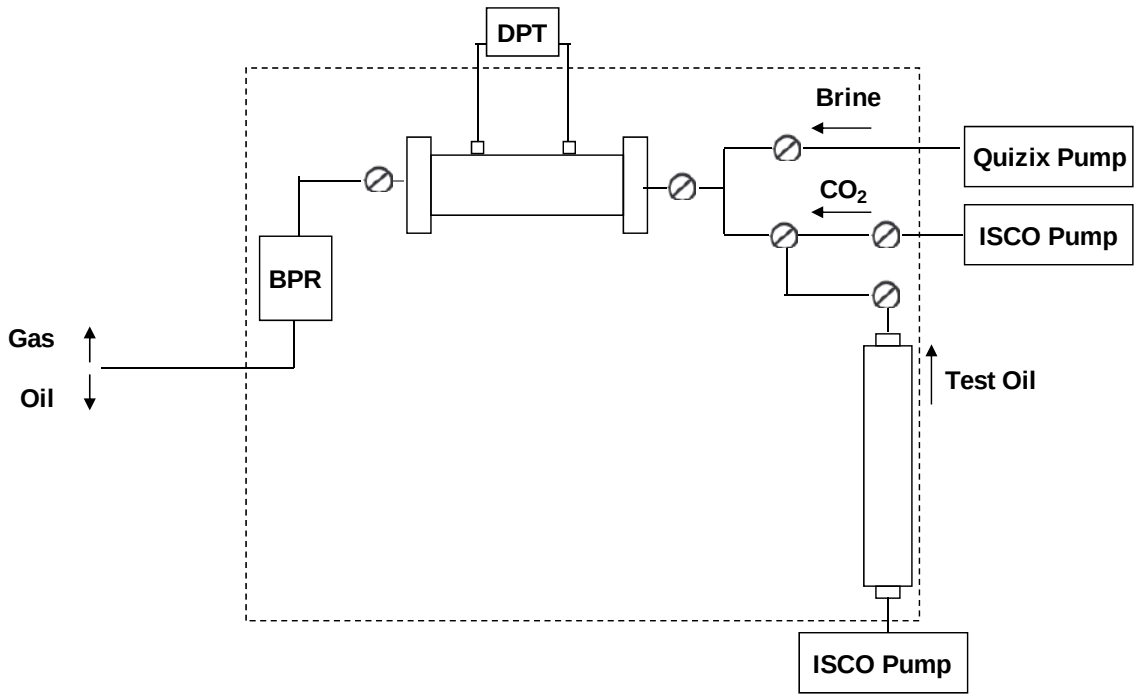

Figure 26 Schematic of core flood setup

The core flood setup is shown in Figure 26. The core flood displacement setup consists of a core holder, injection system, a high-pressure densitometer, a production system and a computerized data acquisition system. The temperature of the system is maintained in a Lindbergh/Blue M oven with Eurotherm temperature control.

The injection system consists of a Parker transfer cylinder (oil storage), two Isco, Inc. 260DM syringe pumps (oil/CO_2 transfer and injection) and a Quizix Pump (brine transfer and injection). The capacity of the transfer cylinder is 485 cc. The cylinder can withstand a maximum pressure of 3000 psi.

The production system consists of a back-pressure regulator, connected to the outlet of the core holder, to set/control the system pressure. Back pressure regulator models BPR-50 is a

dome-load type, which controls the upstream back pressure to whatever pressure is applied to the dome. It is designed to operate using compressed gas in the dome and water, oil, gas in the body. A high pressure bottle of inert gas, such as nitrogen, is required to pressurize the unit. The back pressure regulator has a working pressure of 5000 psi at 200°F (93°C).

During the experiment, the core effluent was flashed to atmospheric pressure at the outlet of the back-pressure regulator. The separator fluid was collected in glassware designed for different stages of displacement. The amount of fluids produced was determined volumetrically and/or gravimetrically.

Three Valydine pressure transducers are installed to measure pressures at different locations, such as pressure drop across the core, upstream pressures (CO_2/oil/brine pressure), and downstream pressure (back-pressure regulator pressure). Pressure drop was recorded during the brine flow test and used to calculate permeability of core sample.

Experimental Procedures

Two sets of core flood experiments were performed, secondary CO_2 flooding and tertiary CO_2 flooding to investigate the effect of operating pressure, in the near-miscible range on the recovery efficiency and to investigate the effect of mobile water on the recovery efficiency. In each set of experiment, core flood tests were carried out for a range of pressures and at the reservoir temperature of 110°F. Crude oil/brine/CO_2 injection volumes were kept the same to compare the amount of oil recovered in each run.

Displacement Rate Selection

Residual oil saturation in laboratory core floods has been observed to depend on CO_2 flow rate. Poorer oil recoveries were found at increasing frontal advance rates by Shelton and Schneider (1975). Low flow rate allows CO_2 to diffuse through the network of pores and hence increase oil recovery by swelling and/or vaporizing. Crude oil/brine/CO_2 displacement rates were selected 0.1cc/min to keep the capillary number as low as 10^{-6} and to achieve realistic unit displacement efficiency in laboratory CO_2 displacement.

Results and Discussions

Table 8 presents the properties of Berea sandstone, Baker dolomite and Arbuckle dolomite. Bulk volumes of the cores were calculated from at least three measurements of

diameters and lengths. Pore volume of each core was averaged from the results of tracer tests and gravimetric methods, and from which porosity of each core was calculated. Permeability to brine was calculated using different flow rates and averaged.

Table 8 Core plug properties

Type	Berea sandstone A1	Berea sandstone A2	Arbuckle dolomite	Baker dolomite
Length (cm)	5.86	14.67	5.97	8.07
Cross section (cm)	2.53	3.86	2.46	2.34
Area (cm^2)	5.01	11.67	4.75	4.30
Pore volume (cc)	5.80	34.72	6.05	7.20
Porosity (%)	19.7	20.28	21.3	20.7
Permeability mD)	238.5	369.04	2.5	89.7

Secondary and tertiary CO_2 flooding experiments were conducted to evaluate the recovery efficiency at operating pressure in the near miscible condition. Injection of CO_2 was controlled at flow rate of 0.1cc/min at operating pressure. The amount of fluid recovered by CO_2 displacement was compared at 6 PV of injection.

Secondary CO_2 Flooding

Berea sandstone was used in this series of experiments with the core saturated with oil prior to injection of CO_2. The recovery efficiency was determined by the amount of oil recovered at 6 PV of CO_2 injections. The recovery efficiency is presented in Figure 27 where the recovery efficiency from slim-tube experiment is also plotted for comparison. The recovery efficiency in a short core was much less than that from slim-tube displacements. The lower recovery at pressure above MMP is probably due to lack of development of multiple-contact miscibility in a short core. At pressure below MMP, the extraction was also less effective as the dispersion is dominated for flow in the core plug as compared to that in a slim-tube. Nevertheless, the density profiles of core flooding effluents showed similarity in density profiles of slim tube effluents at pressure below MMP. Density of effluent during the displacement was higher than density of

pure CO_2 at near miscible pressure. The density behavior of the effluent suggested that the vaporization process took place during core flooding process despite the length of core is short.

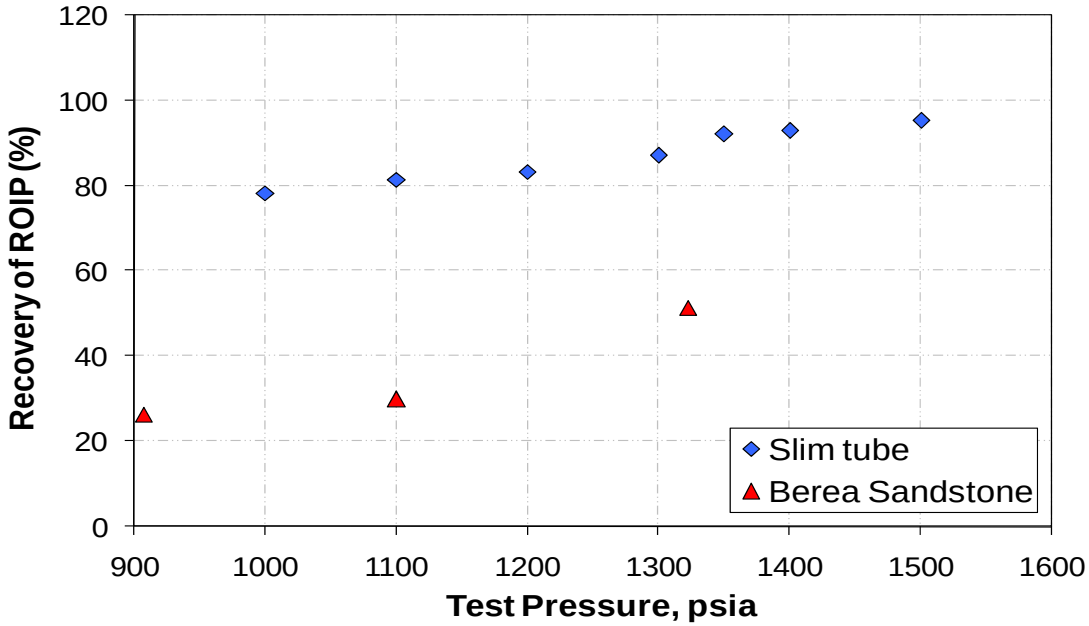

Figure 27 Comparison of oil recovery between slim-tube and core flooding experiment
(Oil recovery @ 6 PV of CO_2 injected in core flow tests and oil recovery @ 1.2 PV of CO_2 injected in slim tube tests at 110°F)

Tertiary CO_2 flooding

Core plugs of Arbuckle dolomite, Baker dolomite and Berea sandstone, were used in this series of experiments. Each core sample was saturated with brine at the test pressure and permeability was measured. The core was then flooded with oil to connate water saturation at flow rate of 0.1cc/min. After connate water saturation was established, the core was water flooded at same rate to residual oil saturation. At least 10 PV of brine and crude oil were used in each sequence of displacement to establish a steady state residual fluid saturation. Carbon dioxide was finally injected to displace the remaining oil in the core. The amount of oil recovered by CO_2 flooding was determined volumetrically. A typical result of CO_2 flooding is presented in Figure 28 where the recovery history of fluid is plotted. Most of recovery occurred before 4 PV of CO_2 injection. No significant fluid recovery was observed after 6 PV of CO_2 were injected.

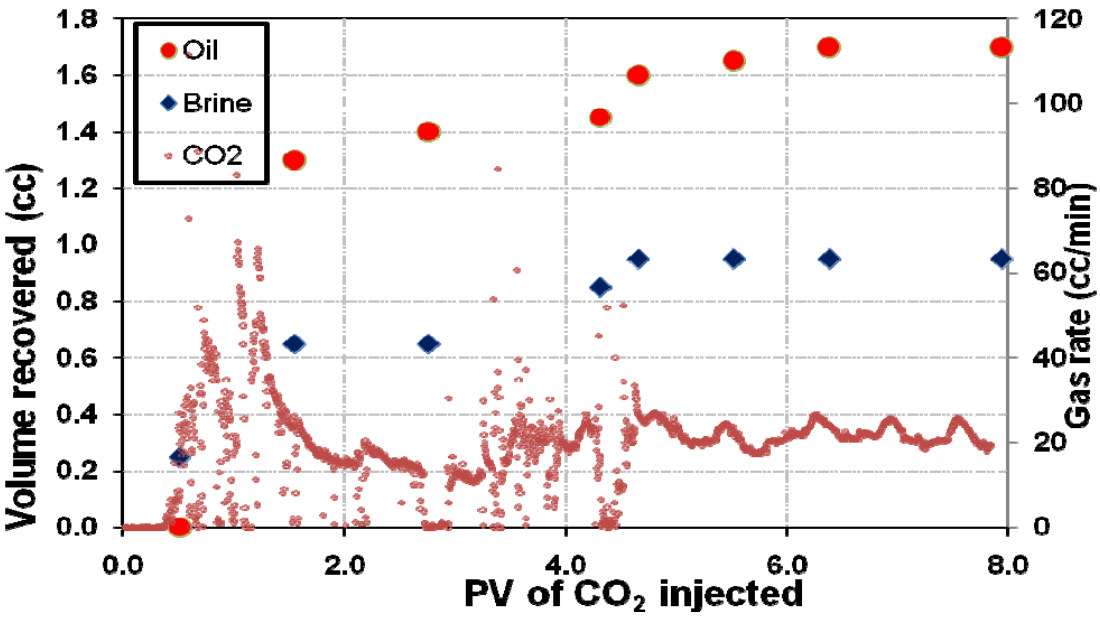

Figure 28 Effluent profile of production fluid during CO_2 flooding at 1317 psig and 110°F

The results of tertiary CO_2 flood in different cores are summarized in Table 9 to 11. Relatively high values of S_{orCO2}, 0.21 to 0.29 were found in Berea sandstone as it had an unusual high S_{orw}, 0.48 to 0.50 prior to CO_2 injections. On the other hand, the S_{orw} of the dolomite core was found to vary from 0.32 to 0.41 with the S_{orCO2} from 0.07 to 0.17 at the near miscible condition. Figure 29 presents the comparison of recovery efficiency among the cores tested. The recovery efficiency of ROIP varied from 60% to 80% for dolomite cores while it varied from 35% to 58 % for sandstone core as pressure increased from 900 psig to 1400 psig. Although the recovery efficiency differed among the rock types, substantial recovery was observed for Arbuckle rock at current reservoir operating pressure of 1150 psig.

Figure 30 gives a comparison of recovery efficiency between secondary and tertiary CO_2 flooding with Berea sandstone. Higher recovery efficiency of remaining oil in place (ROIP) in tertiary CO_2 flooding indicates the existence of water phase is not necessarily detrimental to CO_2 displacement efficiency due to its blocking effect. Instead, the relative permeability of CO_2 at presence of water might be reduced. Coupled with the reduction of the oil viscosity, the mobility ratio between the oil and CO_2 is reduced and therefore the recovery efficiency is improved.

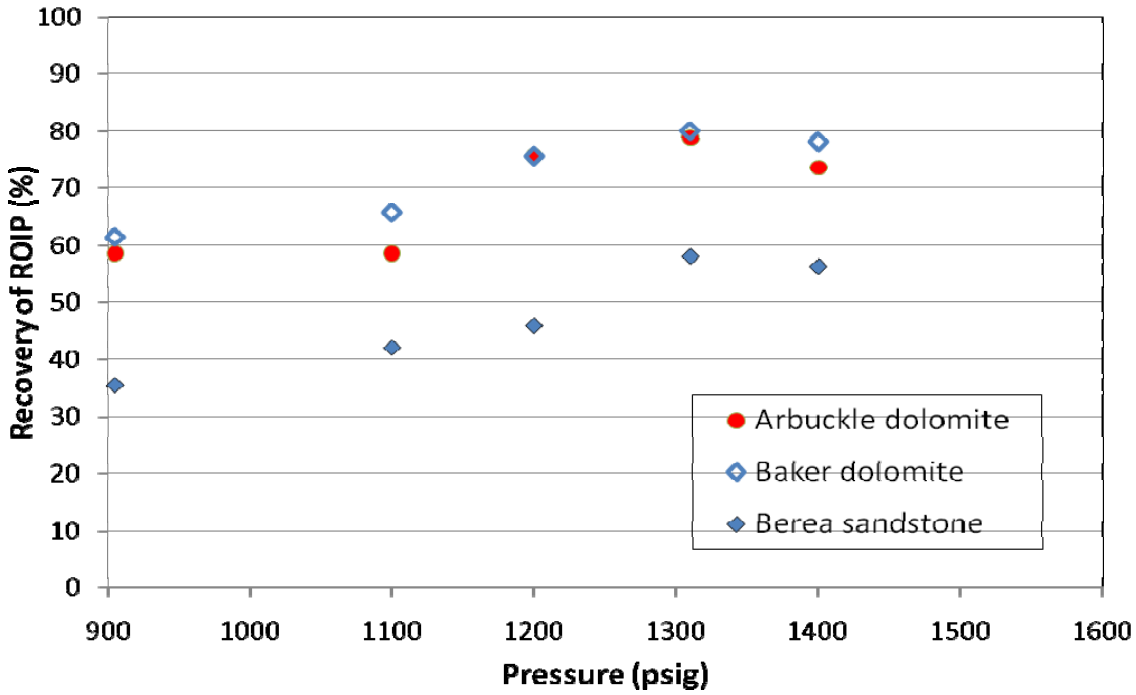

Figure 29 Effect of rock type on recovery efficiency at 110°F

The recovery efficiency was similar between two dolomite cores and was substantially higher than that in Berea core. Wylie and Mohanty (1998) in their study of effect of wettability on oil recovery by gas injection concluded that the mass transfer from the bypassed region to the flowing gas inside a core is enhanced under oil-wet conditions over water-wet conditions. Although the wettability of core was not determined in this study, it is generally believed that Berea sandstone is strongly water wet whereas the dolomite is less water wet. After CO_2 breakthrough from the core, the extraction or the mass transfer between the bypassed region and flowing CO_2 becomes more important to extract the remaining oil inside the core. The findings from Wylie's study may explain why the recovery efficiency is slightly higher in dolomite than that in sandstone tested in this study.

Table 9 Tertiary CO_2 flood results of Berea sandstone

Pressure	S_{wr}	S_{orw}	S_{orco2}	S_{wf}	Recovery $1-(S_{orco2}/S_{orw})$
(psig)					
905	0.318	0.483	0.311	0.370	35.71
1104	0.318	0.500	0.293	0.388	41.38
1198	0.318	0.483	0.259	0.405	46.43
1317	0.318	0.500	0.207	0.336	58.62
1413	0.318	0.483	0.207	0.336	57.14

Table 10 Tertiary CO_2 flood results of Arbuckle dolomite

Pressure	S_{wr}	S_{orw}	S_{orco2}	S_{wf}	Recovery $1-(S_{orco2}/S_{orw})$
(psig)					
901	0.380	0.414	0.165	0.512	60.00
1100	0.380	0.414	0.165	0.553	60.00
1200	0.446	0.331	0.083	0.636	75.00
1305	0.446	0.331	0.066	0.636	80.00
1407	0.380	0.380	0.099	0.529	73.91

Table 11 Tertiary CO_2 flood results of Baker dolomite

Pressure	S_{wr}	S_{orw}	S_{orco2}	S_{wf}	Recovery $1-(S_{orco2}/S_{orw})$
(psig)					
905	0.284	0.389	0.153	0.437	60.71
1109	0.312	0.375	0.125	0.409	66.67
1201	0.340	0.347	0.097	0.451	72.00
1303	0.368	0.347	0.069	0.534	80.00
1402	0.368	0.320	0.069	0.465	78.26

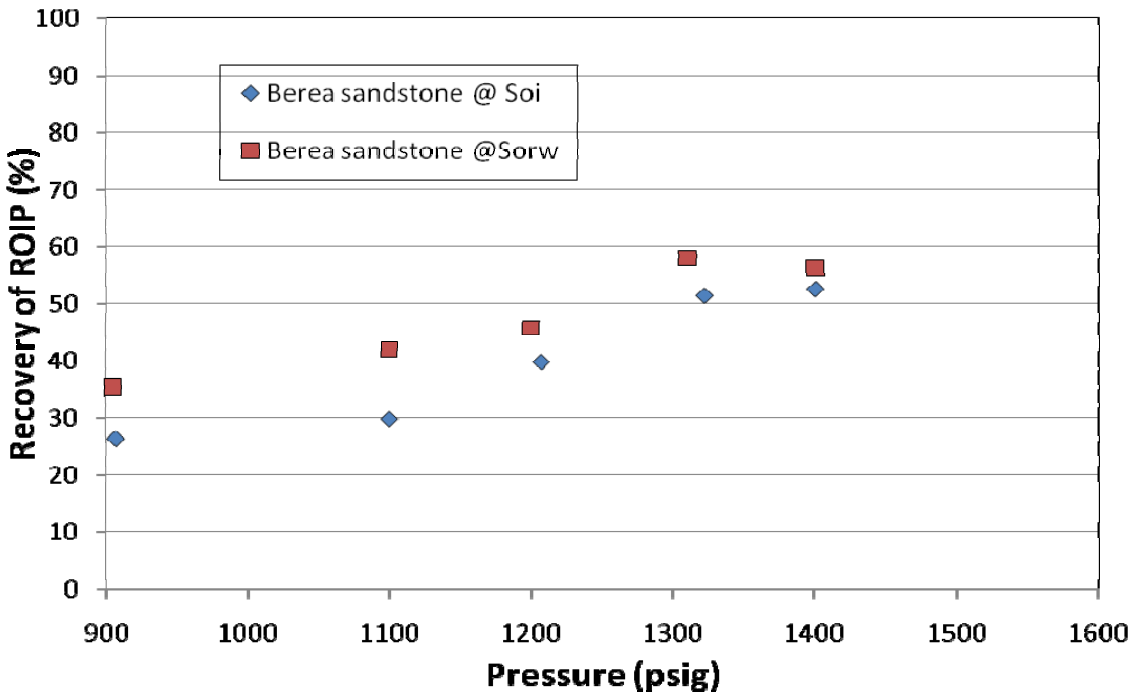

Figure 30 Effect of water saturation on oil recovery efficiency at 110°F

Summary

1) Tertiary oil recovery efficiency varied among rock types, from 65% to 80% for dolomite cores and lesser from 45% to 60 % for sandstone core in the near-miscible region, from 1100 psig to 1350 psig & at 110°F.
2) Recovery of more than 60% of the waterflood residual oil was obtained using Arbuckle reservoir core when CO_2 was injected at the current average reservoir pressure 1150 psig & 110°F.
3) Experimental works showed that the presence of water phase improved the relative permeability of CO_2, which coupled with the reduction of the oil viscosity reduced the mobility ratio between the oil and CO_2 and therefore the recovery efficiency was improved

6. Conclusions

1. Properties of Ogallah unit oil produced from an Arbuckle reservoir in Kansas were determined at reservoir temperature from a series of phase behavior and slim tube experiments where CO_2 was dissolved in or used to displace the oil. The MMP at 110 ºF was 1350 psig. The MMP increased to 1650 psig when the temperature increased to 125 ºF.
2. At near miscible conditions (pressure >1100 psig), the oil viscosity was reduced by a factor of five due to the dissolution of carbon dioxide.
3. Phase behavior data were used to develop an equation of state that correlated properties of carbon dioxide saturated crude oil as a function of pressure at reservoir temperature.
4. Recovery of more than 50% of the waterflood residual oil from Berea, Baker dolomite and Arbuckle reservoir rock was obtained when CO_2 was injected at the current average reservoir pressure of 1150 psig, substantially less than the MMP(1350 psig).
5. Good agreement was observed between simulated and measured oil recovery from slim-tube tests for CO_2 injection over pressures ranging from 1000 psig to 1500 psig.
6. At near miscible conditions, relatively high recovery efficiency in the slim-tube experiment supports extraction/vaporization as a principle displacement mechanism.
7. The swelling of crude oil due to the dissolution of CO_2 was determined accurately in a new apparatus using small sample sizes.
8. The MMP estimated by the swelling/extraction test graphically is close to what determined from the slim-tube experiment.

References

Ahosseini, A. and A. Scurto: "Viscosity of Imidazolium-Based Ionic Liquids at Elevated Pressures: Cation and Anion Effects," International Journal of Thermophysics, 2008. **29**(4): p. 1222-1243.

Jennings, D.W. and R.C. Schucker: " Comparison of High-Pressure Vapor−Liquid Equilibria of Mixtures of CO_2 or Propane with Nonane and C9 Alkylbenzenes," Journal of Chemical & Engineering Data, 1996. **41**(4): p. 831-838.

Hand, J. L. and Plnczewshl, W. V.: "Interpretation of Swelling/Extraction Tests," ***SPERE*** (November 1990) 595-600.

Harmon, R. A. and Grigg, R. B.: "Vapor-Density Measurement for Estimating Minimum Miscibility Pressure," ***SPERE*** (November 1988) 1215-1220.

Negahban, S. and V.J. Kremesec Jr.: " Development and Validation of Equation-of-State Fluid Descriptions for CO_2/Reservoir-Oil Systems*,"* ***SPERE***, 1992. **7**(3): p. 363-368.

Nagarajan, N. and Robinson, R. L. J.: "Equilibrium Phase Compositions, Phase Densities, and Interfacial Tensions for CO_2 + Hydrocarbon Systems, 2. CO_2 + n-Decane," ***J. Chem. Eng. Data***, 31, 168. 1986

Ren, Wei and Scurto, A. M.: "High –Pressure Phase Equilibria with Compressed Gases," Review of Scientific Instruments, 78, 125104, 2007.

Shelton, J.L.: "The Effects of Water Injection on Miscible Flooding Methods Using Hydrocarbons and Carbon Dioxide," 1975. **15**(3): p. 217-226.

Whitson C. H. and Brule M. R.: "Phase Behavior", SPE Henry L. Doherty Series, Monograph Volume 20, Society of Petroleum Engineers, Inc. 2000.

Wylie, P. and Mohanty, K. K.: "Effect of Wettability on Oil Recovery by Near-miscible Gas Injection," paper SPE 39620 presented at the Improved Oil Recovery Symposium, Tulsa, OK. April 19-22, 1998.